

AD-A191 006

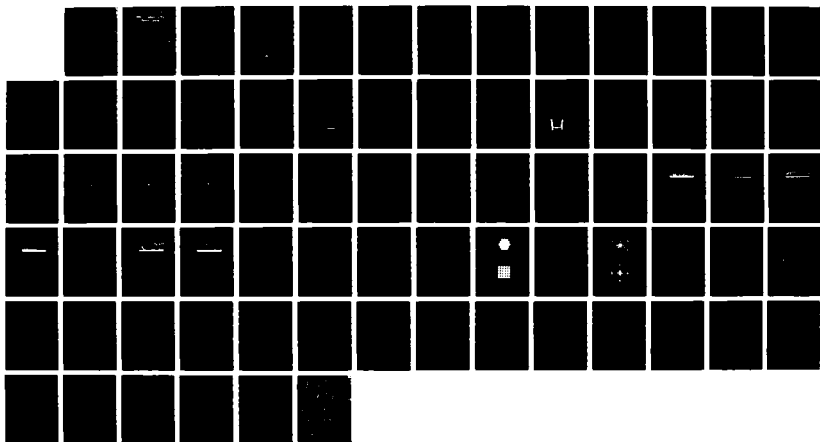
UTILIZATION OF DENSE PACKED PLANAR ACOUSTIC  
ECHOSOUNDERS TO IDENTIFY TUBB. (U) NAVAL POSTGRADUATE  
SCHOOL MONTEREY CA L R MOXCEY DEC 87

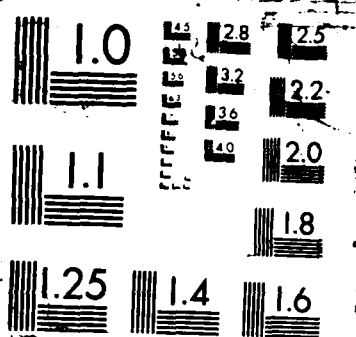
1/1

UNCLASSIFIED

F/G 17/1

NL





AD-A191 006

DTIC FILE COPY

2

# NAVAL POSTGRADUATE SCHOOL Monterey, California



## THESIS

DTIC  
SELECTED  
MAR 24 1988  
S & D  
E

UTILIZATION OF DENSE PACKED PLANAR  
ACOUSTIC ECHOSOUNDERS TO IDENTIFY  
TURBULENCE STRUCTURE IN THE  
LOWEST LEVELS OF THE ATMOSPHERE

by

Louis Robert Moxcey  
December 1987

Thesis Advisor:

D. L. Walters

Approved for public release; distribution is unlimited

88 3 22 039

A191 006

## REPORT DOCUMENTATION PAGE

1a REPORT SECURITY CLASSIFICATION <b>UNCLASSIFIED</b>			1b RESTRICTIVE MARKINGS		
2a SECURITY CLASSIFICATION AUTHORITY			3 DISTRIBUTION/AVAILABILITY OF REPORT <b>Approved for public release; distribution is unlimited</b>		
2b DECLASSIFICATION/DOWNGRADING SCHEDULE			5 MONITORING ORGANIZATION REPORT NUMBER(S)		
4 PERFORMING ORGANIZATION REPORT NUMBER(S)			7a NAME OF MONITORING ORGANIZATION <b>Naval Postgraduate School</b>		
6a NAME OF PERFORMING ORGANIZATION <b>Naval Postgraduate School</b>		6b OFFICE SYMBOL (If applicable) <b>61</b>	7b ADDRESS (City, State, and ZIP Code) <b>Monterey, California 93943-5000</b>		
6c ADDRESS (City, State, and ZIP Code) <b>Monterey, California 93943-5000</b>		9. PROCUREMENT INSTRUMENT IDENTIFICATION NUMBER			
8a NAME OF FUNDING/SPONSORING ORGANIZATION		8b OFFICE SYMBOL (If applicable)	10 SOURCE OF FUNDING NUMBERS		
8c ADDRESS (City, State, and ZIP Code)		PROGRAM ELEMENT NO. PROJECT NO. TASK NO. WORK UNIT ACCESSION NO.			
11 TITLE (Include Security Classification) <b>UTILIZATION OF DENSE PACKED PLANAR ACOUSTIC ECHOSOUNDERS TO IDENTIFY TURBULENCE STRUCTURE IN THE LOWEST LEVELS OF THE ATMOSPHERE (UNCLASSIFIED)</b>					
12 PERSONAL AUTHOR(S) <b>Moxcey, Louis Robert</b>					
13a TYPE OF REPORT <b>Masters Thesis</b>		13b TIME COVERED FROM _____ TO _____		14 DATE OF REPORT (Year, Month, Day) <b>1987, December</b>	
15 PAGE COUNT <b>73</b>					
16 SUPPLEMENTARY NOTATION					
17 COSATI CODES			18 SUBJECT TERMS (Continue on reverse if necessary and identify by block number)		
FIELD	GROUP	SUB-GROUP	Acoustic Echosounders, Atmospheric Turbulence, Fast Fourier Transform Algorithm		
19 ABSTRACT (Continue on reverse if necessary and identify by block number) Coherent light beams propagating through the atmosphere undergo considerable phase perturbations due to fluctuating temperature structures in the atmosphere. Understanding and measuring these structures on a real-time altitude dependent basis is inherent to successful deployment of ground based lasers and particle beams. One method used to detect these temperature structures is an acoustic profiler, or echosounder. Of immediate interest is the ability of high frequency (5 kHz) planar array sounders to rapidly detect low level turbulence (below 200 meters) and quantify the results. This thesis involves design improvements of previously developed echosounder arrays and associated software. Particularly, this thesis demonstrates that tighter packing of elements in a planar acoustic array produces better side lobe reduction than less densely packed arrays. This results in higher energy density in the main lobe and increased performance. Also included in this thesis is a computer method which allows relatively accurate beam pattern prediction from any given planar array.					
20 DISTRIBUTION/AVAILABILITY OF ABSTRACT <input checked="" type="checkbox"/> UNCLASSIFIED UNLIMITED <input type="checkbox"/> SAME AS RPT <input type="checkbox"/> DTIC USERS			21 ABSTRACT SECURITY CLASSIFICATION <b>unclassified</b>		
22a NAME OF RESPONSIBLE INDIVIDUAL <b>Donald L. Walters</b>			22b TELEPHONE (Include Area Code) <b>(408) 646-2267</b>		22c OFFICE SYMBOL <b>61We</b>

Approved for public release; distribution is unlimited

Utilization of Dense Packed Planar Acoustic Echosounders to  
Identify Turbulence Structure in the Lowest Levels of the Atmosphere

by

Louis Robert Moxcey  
Lieutenant, United States Navy  
B.S., Jacksonville University, 1981

Submitted in partial fulfillment of the  
requirements for the degree of

MASTER OF SCIENCE IN PHYSICS

from the

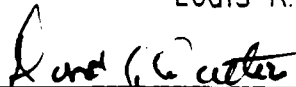
NAVAL POSTGRADUATE SCHOOL  
December 1987

Author:




Louis R. Moxcey

Approved by:



Donald L. Walters, Thesis Advisor



Edmund A. Milne, Second Reader



Karlheinz E. Woehler, Chairman,  
Department of Physics



Gordon E. Schacher, Dean of Science and Engineering

## ABSTRACT

Coherent light beams propagating through the atmosphere undergo considerable phase perturbations due to fluctuating temperature structures in the atmosphere. Understanding and measuring these structures on a real-time altitude dependent basis is inherent to successful deployment of ground based lasers and particle beams.

One method used to detect these temperature structures is an acoustic profiler, or echosounder. Of immediate interest is the ability of high frequency (5 kHz) planar array echosounders to rapidly detect low level turbulence (below 200 meters) and quantify the results.

This thesis involves design improvements of previously developed echosounder arrays and associated software. Particular, this thesis demonstrates that tighter packing of elements in a planar acoustic array produces better side lobe reduction than less densely packed arrays. This results in higher energy density in the main lobe and increased performance.

Also included in this thesis is a computer method which allows relatively accurate beam pattern prediction from any given planar array.



Accession For	
NTIS GRA&I	<input checked="checked" type="checkbox"/>
DTIC TAB	<input type="checkbox"/>
Unannounced	<input type="checkbox"/>
Justification	
By	
Distribution/	
Availability Codes	
Dist	Avail and/or Special
A-1	

## **ACKNOWLEDGEMENTS**

I would like to express my sincere gratitude to Dr. Walters for his outstanding efforts, both as a professor and as an experimentalist. His insight was essential for a successful completion of this thesis.

I would also like to thank my colleague, Lt. Paul Davison, for his friendship and assistance, especially his noted contribution of a polar plotting routine for the Antenna Beam Pattern computer program.

My deepest thanks, though, go to my loving and devoted wife, Nancy. Her patience, understanding and excellent typing were welcome morale boosters during this entire ordeal.

## TABLE OF CONTENTS

I.	INTRODUCTION.....	6
II.	BACKGROUND.....	8
III.	EQUIPMENT.....	14
	A. ELEMENTS.....	14
	B. ARRAY.....	17
	C. ENCLOSURE.....	18
	D. ELECTRONIC HARDWARE.....	19
IV.	RESULTS.....	25
	A. LOBE PATTERNS.....	25
	B. FIELD MEASUREMENTS.....	34
V.	ANTENNA BEAM PATTERN MODEL.....	45
	A. HARDWARE.....	46
	B. SOFTWARE.....	47
	C. RESULTS AND ANALYSIS.....	47
VI.	CONCLUSIONS.....	58
	APPENDIX A LIST OF MATERIAL SOURCES.....	60
	APPENDIX B FAST FOURIER TRANSFORM PROGRAM.....	61
	LIST OF REFERENCES.....	69
	INITIAL DISTRIBUTION LIST.....	72



## **I. INTRODUCTION**

Optical degradation of coherent light in the atmosphere is strongly a function of small scale temperature gradients which change the local index of refraction in the atmosphere [Ref. 1]. These localized structures in the atmosphere fluctuate rapidly, changing in size, density, location, velocity and interaction with neighboring structures. There is also considerable variability with diurnal temperature changes, annual weather variations and regional climatological differences. Understanding the mechanisms of this turbulence and measuring it on a real-time local level are intrinsic to high power earth based lasers.

These small scale turbulence structures in the atmosphere play an even greater role with respect to acoustic absorption and reflection [Ref. 2]. It is well known that acoustic pulses, on the order of 1 to 6 kHz frequency, are ideal in defining turbulence structures in the first few kilometers of the atmosphere, with lower frequencies having greater ranges. Until recently, the most popular type of acoustic sounder was a monopole speaker/receiver mounted in a parabolic dish [Refs. 3 and 4]. Several problems with this method include difficulty of transportation, high amplitude side lobes at large angles and poor altitude resolution due to the low frequencies involved. These deficiencies can be overcome by means of planar arrays [Refs. 5 and 6], and this thesis was designed to amplify this point.

Working under Walters, Weingartner and Wroblewski [Refs. 7 and 8] again demonstrated the feasibility of this technique by building and testing a 25 element 5 kHz planar array. The result was an extremely effective low altitude echosounder which was less expensive, more portable and had better side lobe reduction than previous monopole sounders.

During the course of this previous work several questions arose concerning the planar array. If the elements were more densely packed, then could the size of the side lobes be significantly reduced, thus increasing the accuracy of the beam? Could the array be modeled on a computer to produce the best design? Could the enclosure be improved?

This thesis is an attempt to answer these questions, and involves the development of a dense packed 5 kHz hexagonal array and associated sound deadened enclosure. Additionally, various computer programs using fast Fourier transform algorithms were studied as a first approximation in diagnosing acoustic side lobe suppression.

The results indicate that densely packed planar acoustic echosounders produce better side lobe suppression than more open arrays and are accurate tools in the identification of low level turbulence.

## II. BACKGROUND

The atmosphere induces random phase perturbations on an optical beam. Diffraction of these small scale phase variations produces a larger beam, restricting the ability to focus energy on a target. Optical phase perturbations in the atmosphere stem from temperature fluctuations carried by the turbulent velocity field. These temperature fluctuations vary in size, cascading from tens of meters in diameter down to centimeters and smaller. These structures appear to be most variable and inhomogeneous at the interface between stratified layers, particularly near the earth's surface.

Within the first few hundred meters of the surface, these temperature structures are dominated by the surface heat flux, resulting from differing rates of heat transfer between the earth and the atmosphere. During the day the surface heats much more rapidly and non-uniformly than the atmosphere. An insulating blanket of air near the surface heats and rises off the ground, more or less in sheets. Warmer sections rise more rapidly, quickly disrupting the uniformity of these sheets. Cooler air moves in to replace the rising air, further disrupting the sheets and causing vertical thermal plumes to form. These thermal plumes continue upwards in the atmosphere, slowly mixing and increasing the temperature of the lower atmosphere. This cycle is continuous, with the actual transfer of energy occurring by small scale molecular diffusion. [Ref. 9].

At night the cycle reverses, with the surface cooling off much more rapidly than the air via Planck radiation. In this case, as the air gives up energy to the cooler surface, it produces a turbulent boundary layer (via velocity interaction with a stationary surface) which remains relatively close to the ground. This cooling process is generally less turbulent than the heating process, due to the reduced heat flux at the boundary, although intense turbulence continues to exist at the interface of the horizontally stratified layers.

There is also a neutral event, during the transition between night and day, where the surface temperature equals the ambient air temperature. During this time the net heat flux between the air and the surface changes sign and passes through a minimum. The atmosphere generally becomes optically stable during these brief periods.

The structural variability is clearly evident in optical instruments designed to measure the turbulence of the atmosphere [Refs. 10 and 11], but altitude correlation with optical instruments alone is difficult. Acoustic echosounders alleviate this difficulty.

Acoustic echosounders are devices which generate and propagate energy into the atmosphere and measure the backscatter return from turbulent structures as a function of altitude. The power returned from these turbulent structures,  $P_R$ , is proportional to the power transmitted,  $P_T$ . The equation relating these terms has been summarized by Neff [Ref. 12], based upon work

by Tatarski [Ref 1], and is repeated in equation (1) below.

$$(1) \quad P_R = P_T E_R E_T (ct/2) \{ \exp(-2\beta R) \} (AG/R^2) \mu[R,f] \quad \text{where,}$$

- $P_R$  is the electrical power returned from range  $R$ ,
- $P_T$  is the electrical power transmitted at frequency  $f$ ,
- $E_R$  is the efficiency of conversion from acoustic to electric power,
- $E_T$  is the efficiency of conversion from electric to acoustic power,
- $c$  is the local speed of sound (m/s),
- $t$  is the acoustic pulse length (s),
- $A$  is the antenna area ( $m^2$ ),
- $R$  is the range to the scattering volume (m)
- $\exp(-2\beta R)$  is the round trip power loss due to attenuation where  $\beta$  is the average attenuation to and from the scattering volume,
- $G$  is the effective aperture factor for the antenna,
- $\mu[R,f]$  is the scattering cross-section per unit volume; that is, the fraction of incident power backscattered per unit distance into unit solid angle at frequency  $f$ .

The backscattering cross section,  $\mu$ , is the unknown quantity of interest in Eqn. (1). Tatarski [Ref. 1] uses  $\mu$  in equation (2) (below) to find  $C_T^2$ , the temperature structure parameter.

$$(2) \quad \mu[R,f] = 0.0039 k^{1/3} (C_T^2 / T^2) \quad \text{where,}$$

- $k$  is the acoustic wave number  $= 2\pi / L$ ,
- $L$  is the acoustic wavelength,
- $T$  is the absolute temperature and
- $C_T^2$  is the temperature structure parameter.

The temperature structure parameter,  $C_T^2$ , is the mean squared temperature difference between separate points in space,

$$(3) \quad C_T^2 = \{ \langle T_2(R_2) - T_1(R_1) \rangle^2 \} / (R_2 - R_1)^{2/3} ,$$

and provides the scattering centers which produce backscattered energy from the turbulence.  $\langle \Delta T \rangle^2$  empirically increases by  $\Delta R^{2/3}$ . Therefore, it is normalized by  $\Delta R^{2/3}$  to produce a relatively constant temperature structure parameter.

Since  $\mu$  is proportional to the backscattered return power,  $P_R$ , and to the temperature structure parameter,  $C_T^2$ , then  $P_R$  is proportional to  $C_T^2$ . Solving equation (1) for  $\mu$  and equating equations (1) and (2), the following expression for  $C_T^2$  is given for an acoustic echosounder of wavelength  $L$ ;

$$(4) \quad C_T^2 = 1/0.0039 (1/E_R E_T) T^2 k^{-1/3} (2/ct)(1/AG) P_R/P_T \{R^2 \exp(2\beta R)\}.$$

The electric to acoustic efficiency factors for the transducers (speakers) were measured in Reference 7 and are inherent to the design of the speakers.  $E_R \approx E_T \approx 0.5$ , an excellent value for speaker efficiency, which accounts for their use. The aperture area,  $A$ , for the 19 element hexagonal array is 0.0866  $m^2$ .

The effective aperture factor for the array,  $G$ , accounts for the non-uniform antenna directivity.  $G$  is a difficult quantity to calculate or measure. It represents a normalized average of the acoustic energy within the transmit/receive antenna beam lobe and is clearly summarized by Probert-Jones [Ref. 13].

Based upon Reference 13 and studies by Hall and Wescott [Ref. 14], a value of  $G = 0.4$  is currently used in computations. This quantity is presently undergoing extensive research by Dr. Walters.

Another difficult factor in Equation (4) involves the average atmospheric attenuation loss factor,  $\beta$ , which is strongly dependent upon frequency and the absolute water vapor in the atmosphere [Refs. 2 and 15]. This dependence is illustrated in Figure 1, which is taken directly from Reference 15. The water vapor pressure is measured via a digital humidity/temperature indicator, model 5165-A from Weathermeasure [Appendix A].

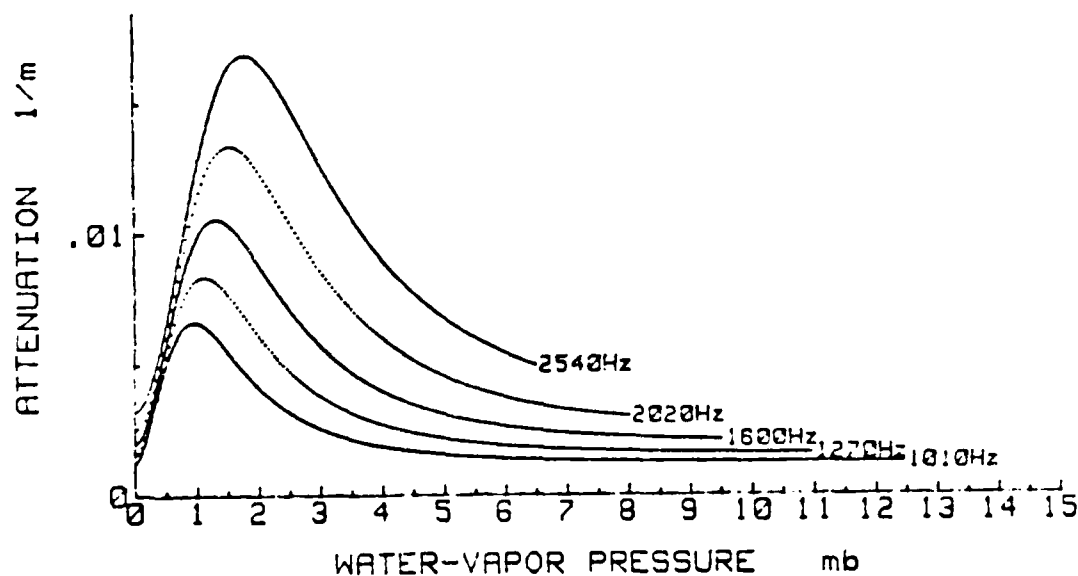


Fig. 1. Attenuation versus Water-vapor Pressure (mb.) for Frequencies around 1.6 KHz.

Combining these known values into a constant Q, equation (4) becomes;

$$(5) \quad C_T^2 = (Q) T^2 k^{-1/3} \{P_R / (ct)(P_T)\} R^2 \exp(2\beta R) \quad \text{where,}$$

$$Q = \{2P_R\} / \{0.0039 P_T E_R E_T A G\}.$$

Wroblewski [Ref. 8] utilizes this in the software for the echosounder to calculate a 15 minute time averaged value for the temperature structure parameter as a function of altitude. Uncertainties in the antenna beam shape, side lobes, rejection, electronic gains, transducer efficiencies, electronic antenna gains and the atmospheric attenuation produce uncertainties in the absolute calibration of an echosounder.

Independent verification of the  $C_T^2$  values measured and calculated by the echosounder are necessary to confirm the accuracy of this technique. Without this confirmation it is still possible to gauge relative variations in the low level turbulence, simply with the echosounder profiles. These profiles are presented and discussed in the following chapters.



### III. EQUIPMENT

Much of the equipment used in this project was borrowed from the 25 element square array designed by Weingartner and Wroblewski. The equipment basically involves a Hewlett Packard (HP) 217 computer for data generation and analysis, an HP 3314A function generator (controlled by the software) which produces the initial pulse, an amplifier, a switch/pre-amp which passes the initial pulse then amplifies and transfers the return signal to the computer, the array and shroud which act as the physical transmitter/receiver and a filter used to eliminate stray noise. These units will be broken down and individually discussed in this section. The software developed for the echosounder by Wroblewski was not significantly altered and is not included in this document.

[Refs. 7 and 8]

#### A. ELEMENTS

The elements of the array consist of 19 piezoelectric Motorola brand speakers, model # KSN 1005A, with attached horns of model # KSN 1032A. Ceramic piezoelectric drivers were chosen

because of their small size, excellent (see Figure 2 ) frequency response at 5 kHz, and a shorter 'ring' time with respect to electrodynamic speakers. Any speaker acts as a damped harmonic oscillator with a 'ring' time (recovery time) inversely proportional to the damping constant. The damping is much stronger in Piezoelectric speakers than in conventional electrodynamic elements.

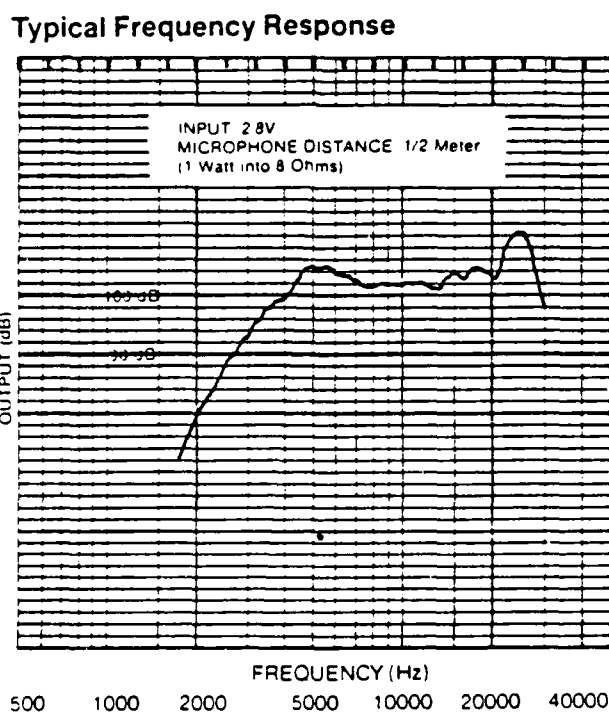


Figure 2. Speaker Frequency Response

An initial set of 40 speakers was tested to find 19 which were similarly matched in frequency response. This testing was done by comparing the output of a chosen reference speaker with the acoustic-to-electrical conversion of each test speaker. By clamping the reference speaker face-to-face with the test speaker, a known voltage to the reference should produce a range of voltages from the test specimens. These voltages were compared using Lissajous plots on a Nicolet Oscilloscope. It was more important to obtain a set of identical speakers rather than the best speakers, in order to achieve a more uniform final array.

The horns on each driver, originally circular with a square flange face were trimmed to a circular diameter of 7.62cm such that they fitted close packed. Ideally a diameter of  $d = L/2$  ( $L$ =wavelength) would provide optimal phase spacing of elements, but this required either smaller speakers ( $d \approx 3.4$  cm) which were unavailable, or a lower frequency ( $\approx 2230$  Hz), which was below the useable range of available speakers.

Another source of speaker was identified as a Philips brand piezoelectric 2002 PI [Ref. 16] with better frequency response at

3kHz than the Motorola speakers in use. Unfortunately these Philips speakers are no longer manufactured.

## B. ARRAY

The speaker elements were configured in a close-packed planar array on an aluminum-covered balsa wood board to absorb vibrations (Fig. 3). The elements were wired in parallel, reducing the array impedance to  $300 \Omega / 19 = 15.8 \Omega$ . The mounting box was locally constructed of sheet aluminum and enclosed a layer of semi-porous foam loaded with a thin lead sheet to reduce stray noise signals. Input/Output was via a coaxial connector. Bracketts were attached to allow 360° rotational testing from 2 axes in the anechoic chamber.

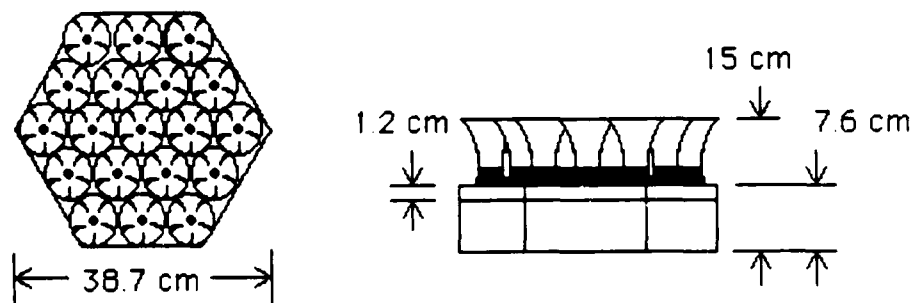


Figure 3. Array Dimensions

### C. ENCLOSURE

The enclosure was designed to be easily reproducible, inexpensive, portable, and easily assembled [the earlier enclosure took some time to set up and break down]. Optimally, a long cylindrical enclosure was desired to reduce side lobe scatter and return without obstructing the main lobe. The enclosure chosen to optimize the above requirements was a Rubbermaid 55 gallon plastic trash container, with a height of 84 cm, having a slight upward taper; the barrel has a lower inside diameter of 53 cm, opening to a diameter of 60 cm. This provided a finished open half angle of about  $20^\circ$ ,  $8^\circ$  more than optimally desired according to tests in the anechoic chamber with the unencumbered array [see RESULTS]. A second possibility was a highway barrier barrel [Appendix A], but these were much more expensive and involved similar dimension problems.

The inside surface of the enclosure was covered with lead lined semi porous foam, with 7.62 cm convoluted (egg crate shaped) foam on one side, and 2 cm flat foam on the backing side. The entire foam

liner was attached with standard contact cement. The lead lining amounted to a density of about 1 lb/sqft which is sufficient to reduce one way noise penetration by 40dB. The convoluted foam helped break up internal and off axis scatter (spectral reflection) and aided in side lobe reduction. The foam used turned out to be the last of a salvage batch of foam, and a second source of foam was desired. An ideal substitute for lead lined foam (which was difficult to obtain) was found to be a barium impregnated vinyl foam (a thin rubbery vinyl layer loaded with barium and sandwiched between semi-porous foam) with a similar density of 1 lb/sqft and virtually identical sound absorption capability (40dB). Two sources of this foam were identified [Appendix A].

#### D. ELECTRONIC HARDWARE

The data processing system consisted of an HP Model #217 computer with a 20 megabyte hard drive and 2 megabyte memory, an INFOTEK BC 203 Basic compiler, analog to digital (A to D) converter, INFOTEK FP 210 floating point accelerator (to enhance the speed of execution), HP 9133 floppy disk drive, monitor and HP ink-jet

printer (see Figure 4). The HP 217 was the workhorse of the system, triggering the function generator, receiving and processing the return pulse, and outputting the results in graphical mode. Without this unit, timely acquisition and reduction of data would be impossible.

The HP 3314A function generator, adjusted and triggered automatically by the HP 217 computer, was used to generate a specific transmitted signal. This signal was generally 100 cycles of a sinusoidal waveform of 1.5 volts (rms) amplitude.

A QSC model 1700 audio amplifier was used to increase the voltage to the array from 1.5 volts (out of HP 3314A) to 30 volts (rms). This model was chosen because of its ability to drive a highly reactive load (the array). A lighter, more compact amplifier could easily replace this item of equipment, and will be considered during future upgrades.

A pre-amplifier (pre-amp) (Fig. 5) was used to isolate the transmitted pulse from the received pulse and to amplify the return signal by a gain of approximately 11,000. The pre-amplifier was

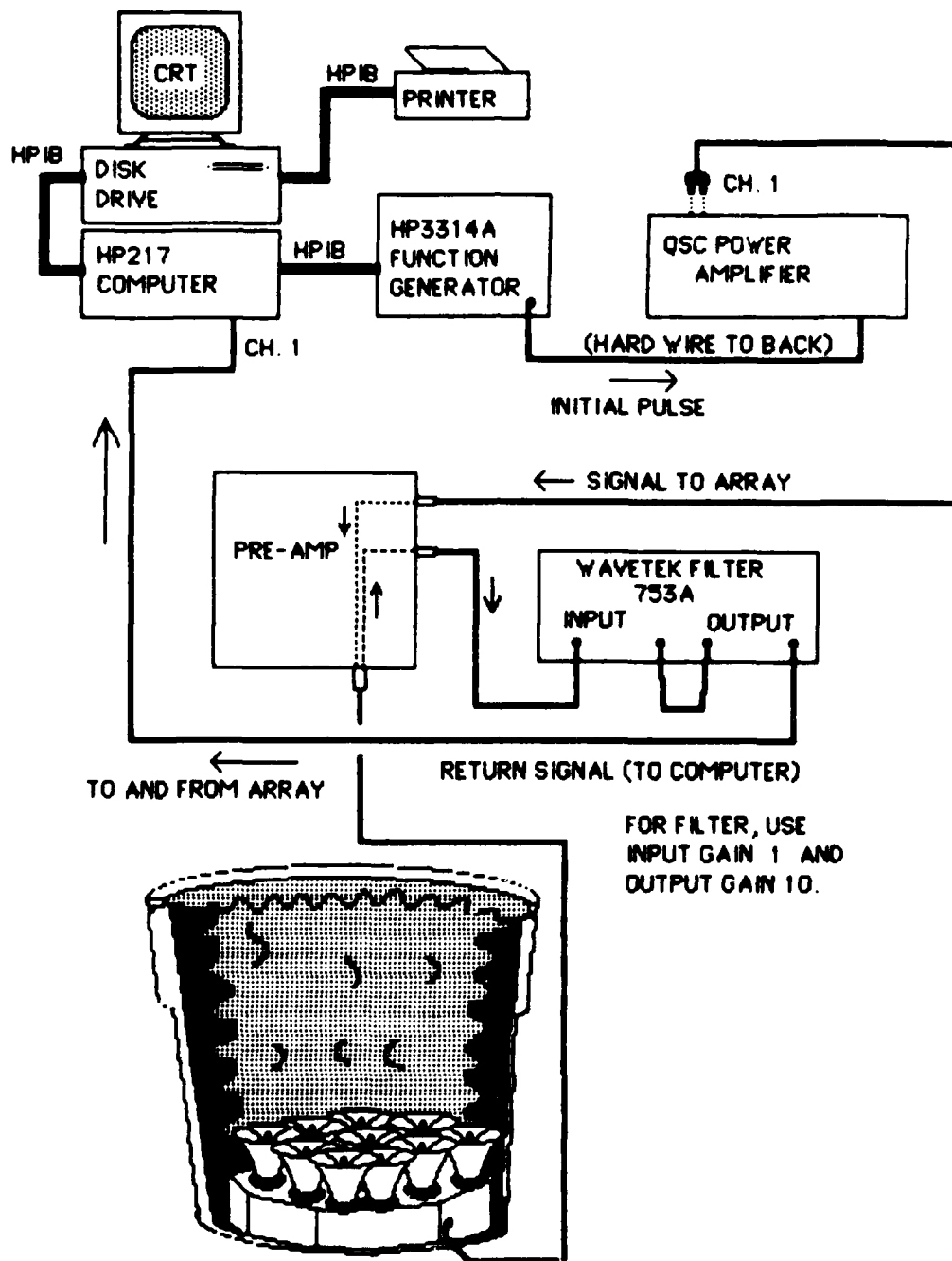


Fig. 4. Echosounder System Set-up.



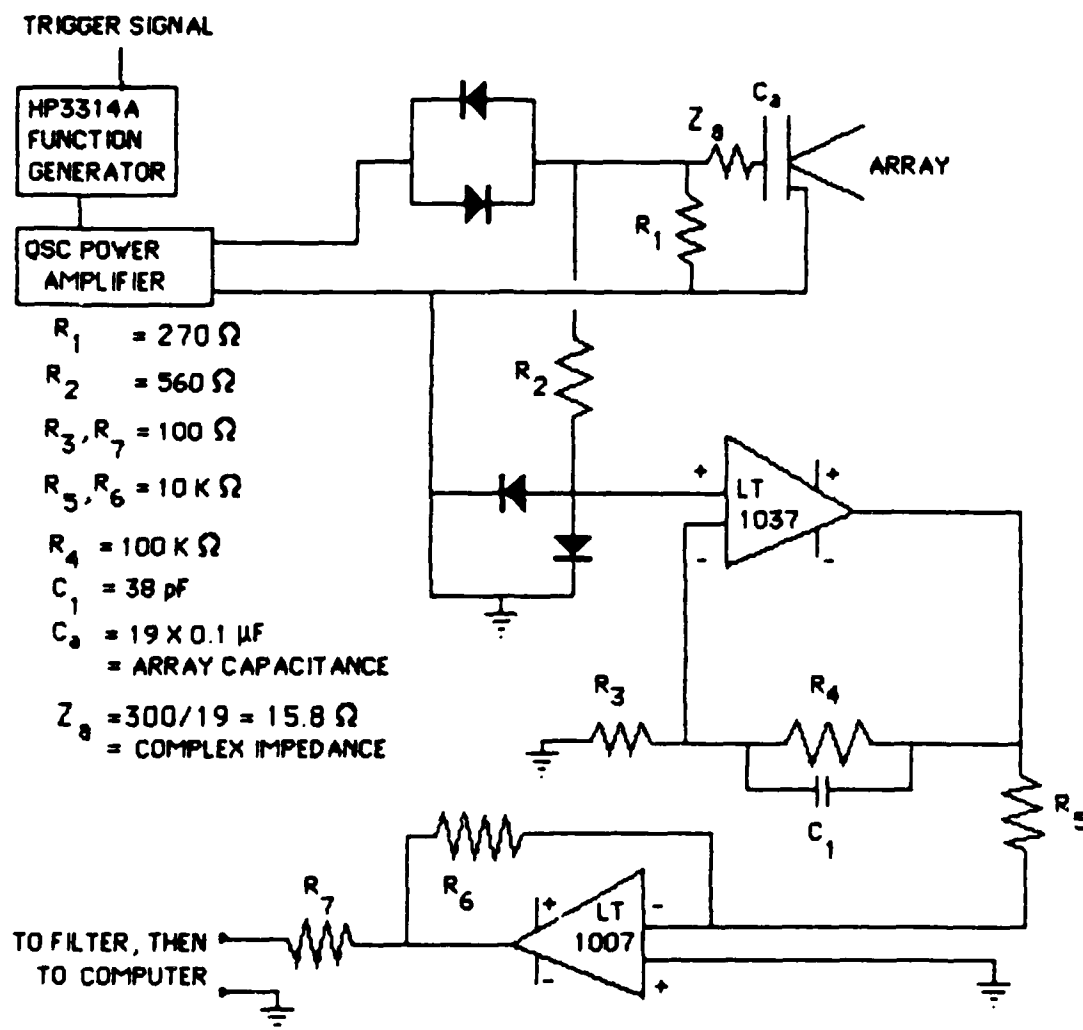


Fig. 5. Schematic of Pre-Amplifier

designed and built by Walters and utilizes two low noise solid state operational amplifiers, an LT 1007 and LT 1037. All four isolation rectifiers were of type IN 4000.

The important properties to consider for an effective pre-amp were complete isolation of the circuit during transmission (to prevent overloading components) and immediate signal retrieval following the 'ring' time of the array. The more rapid the recovery time of the array (a function of driver capacitance ( $C_a$ ) and the loop resistance ( $R_1$ )), the quicker the pre-amp can respond to returned signals and the smaller the surface blind zone. For this array, the capacitance of each driver was  $C_D \approx 0.1 \mu F$ . Thus the time constant for the array was

$$\begin{aligned} RC &= (C_D)(\#drivers)(R_1) = \text{time constant} \\ &= (0.1 \cdot 10^{-6} F)(19)(270 \Omega) = 0.513 \text{ msec.} \end{aligned}$$

For a given array, resistor  $R_1$  provides the time constant of the circuit.

After 5 time constants there is virtually no 'ringing' left on the array, and this sets the minimum height of the blind zone. Thus:

$$5 \times T = 2.57 \text{ ms} \quad \text{and} \quad H_{\min} = (340 \text{ m/s})(5.32 \times 10^{-3} \text{ s}) \approx 0.87 \text{ meters.}$$

Therefore the blind zone stands at approximately 1 meter above the array, which is not noticeable on the echosounder printout.

A Rockland Wavetek model #753A filter {115 dB/octave} was used to isolate noise and further amplify the return signal prior to computer analysis. The input side of the filter was set up as a low pass filter at 5 kHz and gain setting of 0 dB (x1); the output side was set up as a high pass filter at 5 kHz with a gain setting of 20 dB (x10). This produced a band pass filter centered at 5 kHz with a band width of about 100 Hz at the -3 dB level. The over all gain of the filter in this mode was measured as

$$\frac{\text{output}}{\text{input}} = \frac{685 \text{ m volt}}{70.88 \text{ m volt}} = 9.67 \approx 10$$

The combination of the pre-amp and the filter produced an overall return signal gain of  $(\text{pre-amp gain})(\text{filter gain}) = (11094)(9.67)$   
 $\approx 107,000.$

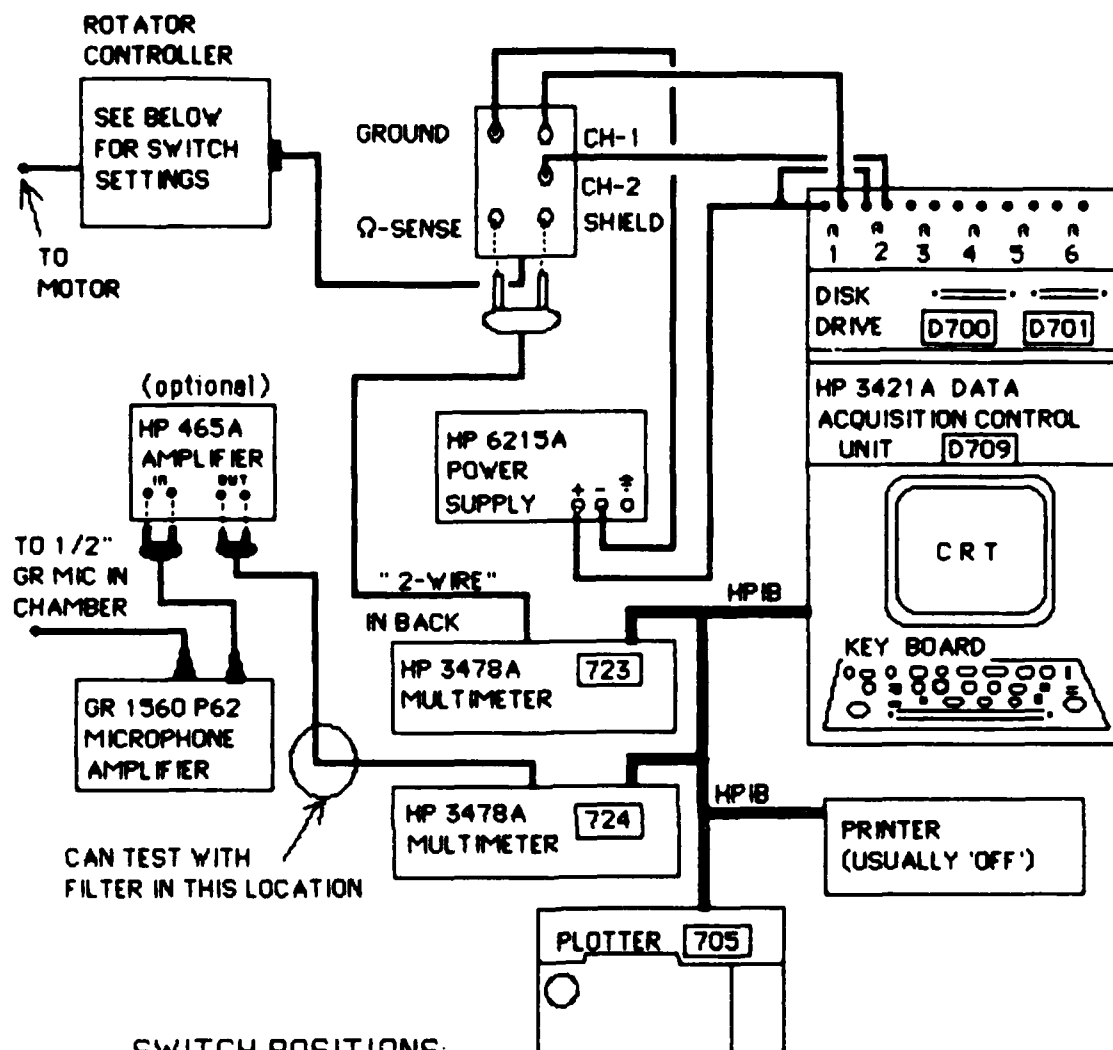
The gain of the system is thus:  $107,000 * 270 \Omega / (270 + 15.8 \Omega)$   
 $\approx 101,000.$

## IV. RESULTS

### A. LOBE PATTERNS

The array was tested in the anechoic chamber utilizing a program designed by Butler [Ref. 17]. This program utilizes the set-up shown in Figure 6 and allows the measurement of beam patterns for various arrays. A band pass filter was used to increase gain and reduce 60 Hz noise from the equipment. Present on all the lobe patterns is a spurious lobe at  $\approx 135^\circ$ . This was determined to be a reflection from the inside door handle of the anechoic chamber and should be ignored. All lobe patterns have been normalized to the maximum voltage detected, allowing easy comparison between figures.

The hexagonal array was rotated around two axes to obtain the maximum sidelobe field of the array (Figs. 7 and 8). The pattern for the square array is shown for only one axis of orientation (Fig. 9). Comparison between the two arrays (Figs. 7 and 9) shows a definite decrease in side lobe number and intensity for the hexagonal array versus the square array.



# SWITCH POSITIONS:

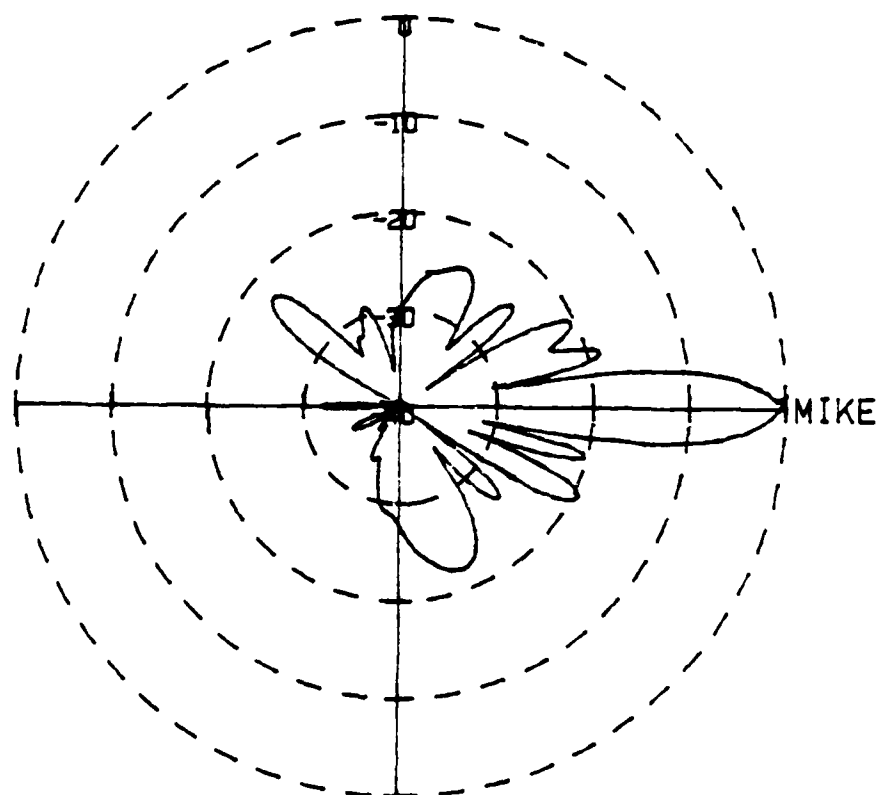
ROTATOR CONTROLLER: BATT IS "OFF"; CCW/"CW"; ON/"OFF"  
FULL SCALE/ZERO/"OPERATE"

723: SET TO READ 'OHMS' (2WIRE  $\Omega$ ); ADJUST THE ARRAY SO  
THIS STARTS IN THE "OYLD" (OVERLOAD) POSITION

724: SET TO READ "VOLTS AC" ( $\sim V$ ).

Figure 6. Anechoic Chamber Set-up

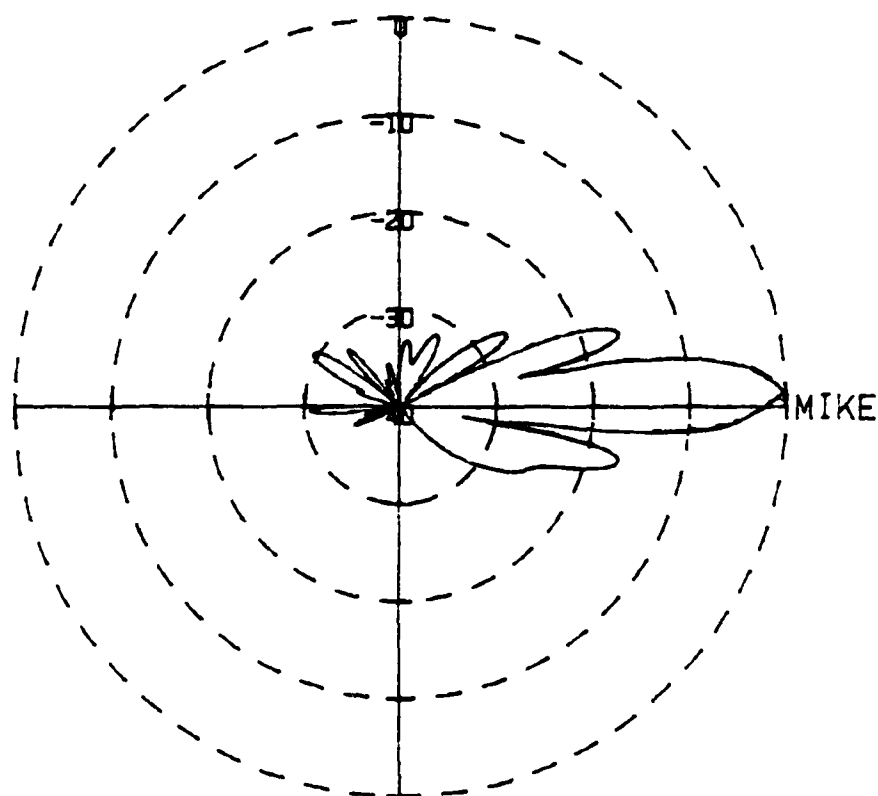
# 19 ELEMENT HEXAGONAL ARRAY - APEX MOUNTED



RUN 97    MIKE= 6.2838 V    INPUT=2.5 V    FREQ=5050 HZ    FILTERED

FIG. 7.    HEXAGONAL ARRAY BEAM PATTERN - APEX MOUNTED

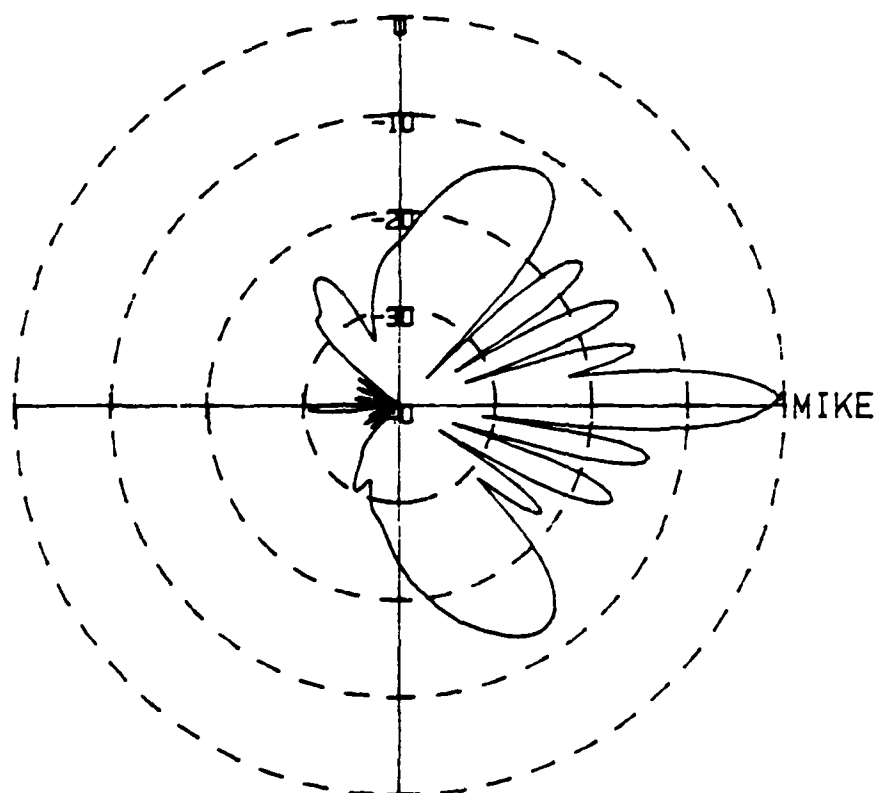
# 19 ELEMENT HEXAGONAL ARRAY - SIDE MOUNTED



RUN 90 MIKE= 6.4951 V INPUT=2.5 V FREQ=4950 HZ 355 PTS FILTERED

FIG. 8. HEXAGONAL ARRAY BEAM PATTERN - SIDE MOUNTED

# 5 X 5 ACOUSTIC ARRAY BEAM PATTERN



R=3.60 M    MIKE VT= 8.2465    INPUT=5.0 V    FREQ=5.0 KHZ

FIG. 9.    SQUARE ARRAY BEAM PATTERN - SIDE MOUNTED



While the array was being tested in the anechoic chamber a demonstration of its detecting ability was desired. Using a heat gun, the array was set up in the chamber exactly as it would be in the field, except a Nicolet model #3091 digital Oscilloscope was used to detect the return signal.

The heat gun was tested at three different settings; first was 'heat and air', then 'air only' and last 'heat only'. With the heat and air both on, a definite fluctuating signal could be detected on the oscilloscope screen. With 'air only' there was virtually no detectable signal and with 'heat only' the signal was almost back to its level of 'heat and air'. No measurements were taken, but the demonstration was repeated several times. This directly illustrated that the turbulence structures in the atmosphere are mainly a result of temperature fluctuations and not due to turbulent velocity fluctuations.

The next step involved testing the side lobe suppression of the enshrouded array. The mechanics of this operation were considerably more involved than simply suspending the array from a rotating motor. Being too heavy to suspend, the shroud was taped to

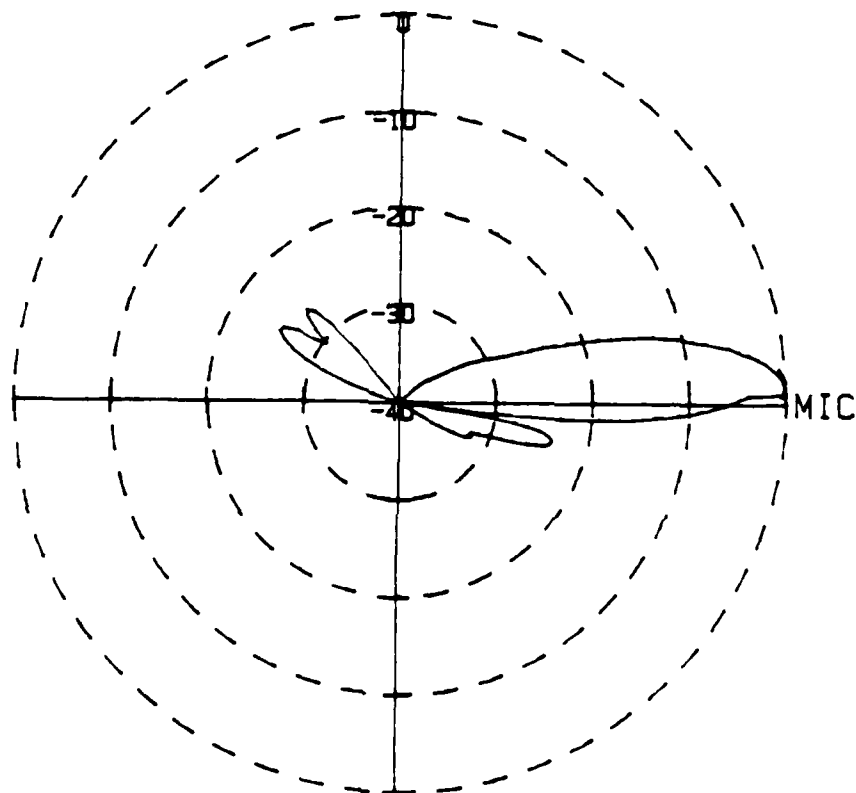
a rotating turntable and centered beneath the rotator motor. The motor was connected to the shroud via aluminum rods and clamps. When the rotating motor turned, so did the shroud, allowing the enshrouded beam pattern to be measured and recorded with the same software as used previously.

The initial beam pattern, (Fig. 10) showed that the shroud, while significantly *reducing* side lobes, was not long enough to completely eliminate them. Some of the side lobes were getting through.

A first-cut step in further reducing these side lobes involved placing a 15 cm wide sleeve of barium impregnated smooth foam around the upper inside circumference of the shroud. The result (Fig. 11) was not promising, and demonstrated that further refinement was required. One thing Figure 11 demonstrated, however, was that specular reflection from a smooth surface increases side lobe activity and thus convoluted foam shrouds (vice smooth foam shrouds) are required.

The next step involved placing a 15 cm wide annular ring coated with sound deadening foam over the exit of the shroud (similar to a trash can lid with the center removed). This left an open circle of

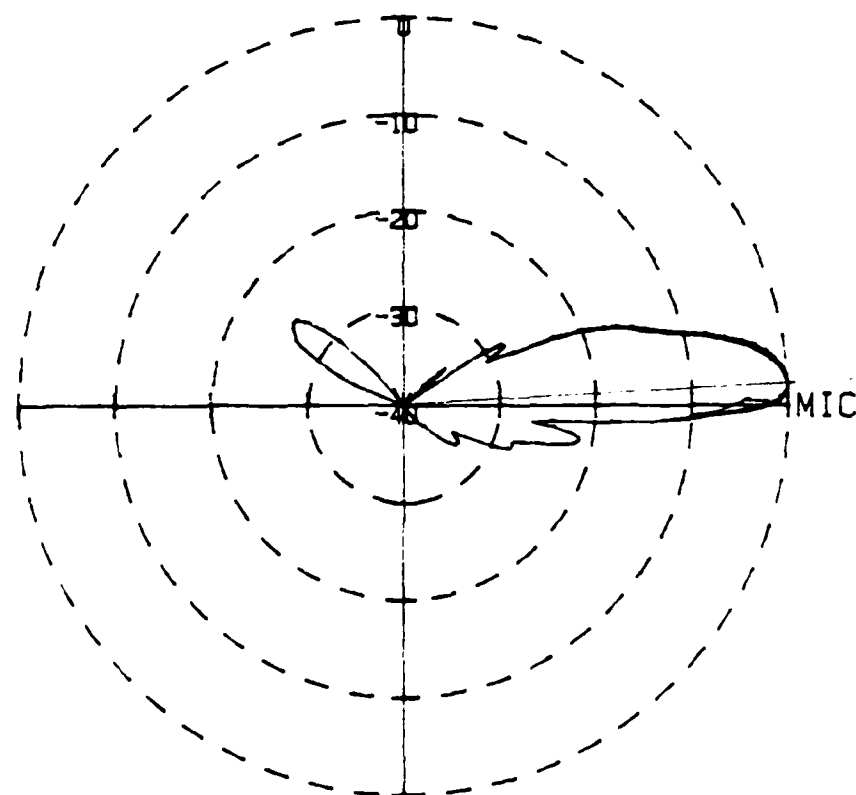
ENCLOSED - HEXAGONAL ARRAY - FILTERED



RUN 115 MIC = .157885 V INPUT=2.5 V FREQ=5000 HZ

FIG 10. ENSHROUDED ARRAY

ENCLOSED - HEXAGONAL ARRAY - FILTERED



RUN MOD1 MIC = .114418 V INPUT=2.5 V FREQ=5000 HZ

FIG. 11. ENSHROUDED ARRAY WITH RING LINER

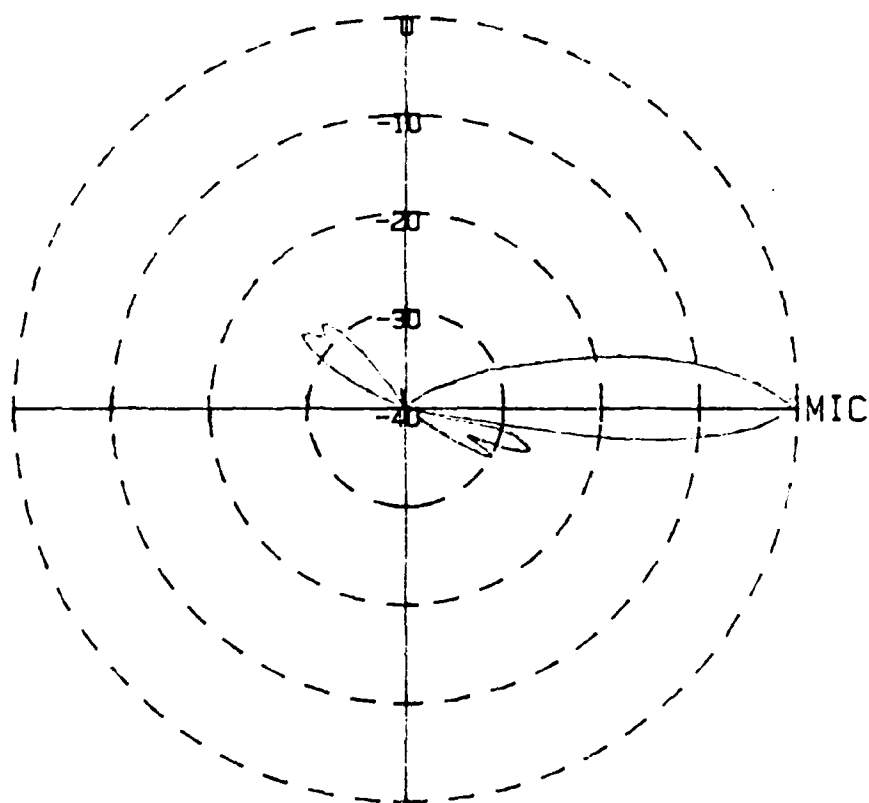
48.25 cm diameter for the acoustic waves to propagate. This adjustment slightly decreased the side lobes ( $\approx 3$  dB), but not significantly (Fig. 12). Further narrowing of the neck via more annular rings only succeeded in reducing the main lobe, with little subsequent change in side lobe activity.

## B. FIELD MEASUREMENTS

Field measurements were conducted on several occasions over a six month period at various locations around California. They generally coincided with optical measurements being conducted by Walters [Refs. 9 and 10] and were used to supplement the optical data. Of greatest interest were mountaintops above the marine boundary layer ( $\approx 4000$  ft.), where the turbulence should be a minimum.

Two mountaintops in particular were visited, one being Lick Observatory on Mt. Hamilton and the other being Mt. Wilson Observatory at Mt. Wilson. These were chosen because of the availability of telescope domes, which were required to reduce wind vibration on the optical components and protect the computers from

ENCLOSED \* HEXAGONAL ARRAY \* FILTERED



RUN MOD28 MIC = .140021 V INPUT=2.5 V FREQ=5000 HZ

FIG 12. ENSHROUDED ARRAY WITH ANNULAR MUZZLE

dust and debris. The echosounder itself is impervious to wind, and can be operated wherever electricity is available.

Lick Observatory was visited on 1 and 2 August 1987 and some of the results are presented in the following figures. All times are given as universal time. Subtract seven hours to obtain local (daylight savings) time at the site. Both days were similar with respect to turbulence. Therefore, only profiles from 2 August will be presented to illustrate the ability of the echosounder to detect and present the rapidly varying nature of the atmosphere accurately. The  $C_T^2$  profiles are currently unverified and should be ignored.

Figure 13 was taken early in the evening and demonstrates the presence of convective pluming. This pluming vanishes gradually, eventually yielding to the nighttime structure which starts in Figure 14. By this time a definite layer has set in and surface pluming is no longer dominant. Later in the evening a strong turbulence layer descends (Fig. 15) which quickly settles [Fig. 16] and is quite dense. This layer remains close to the ground the rest of the evening, with light turbulence detectable above it.

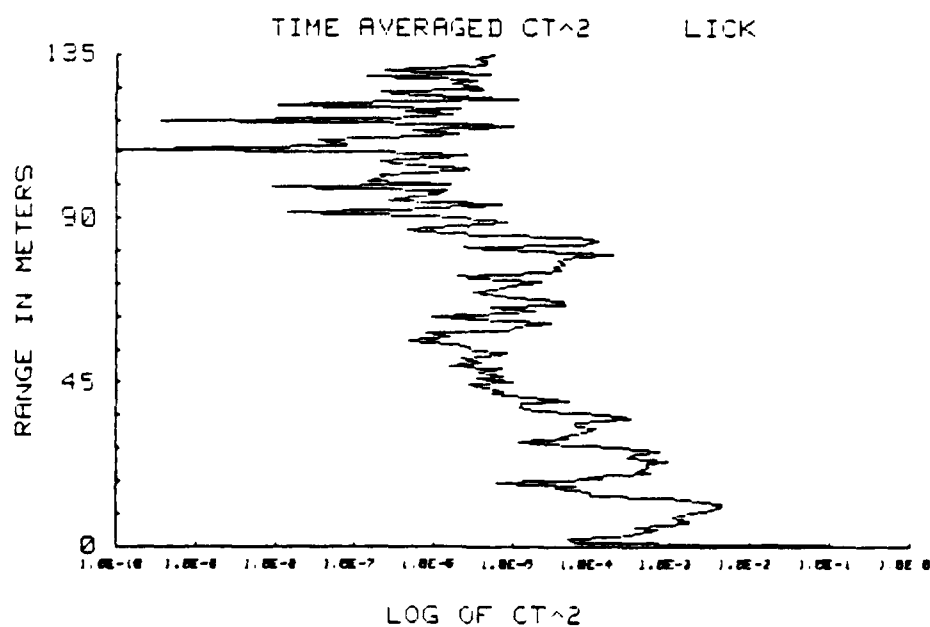
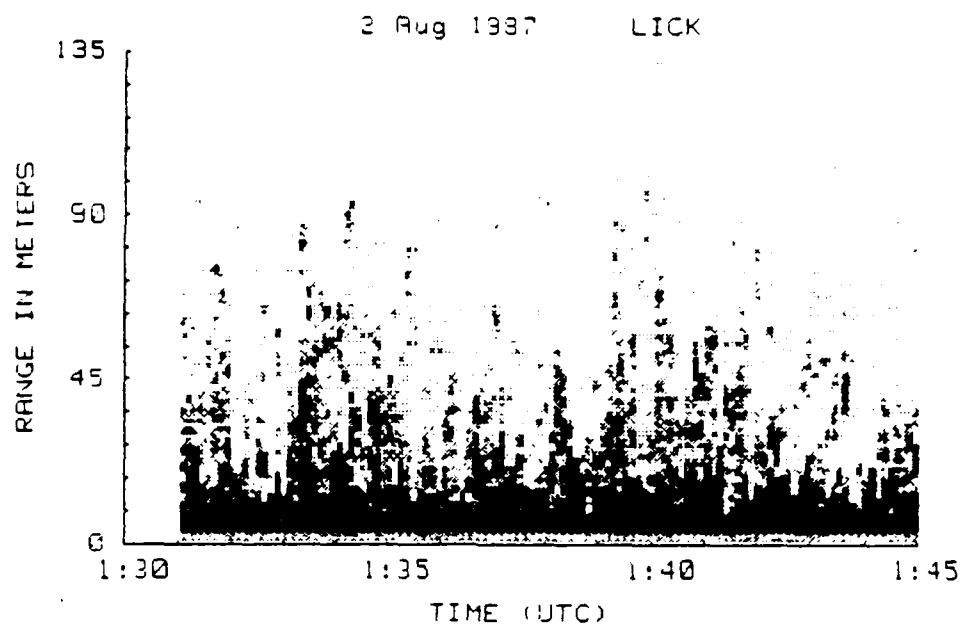


Fig. 13. Echosounder Profile; 1830 - 1845 Local Time



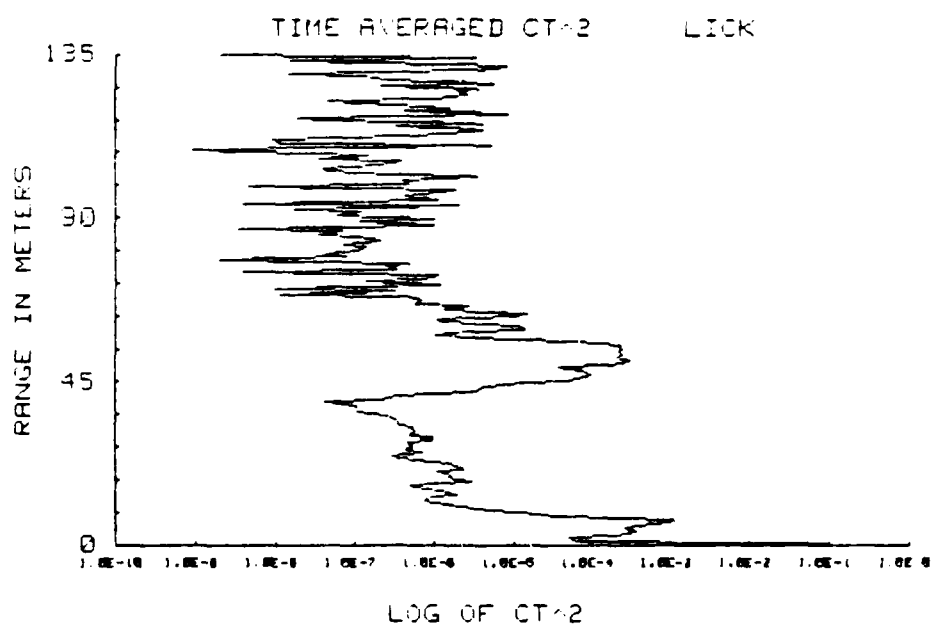
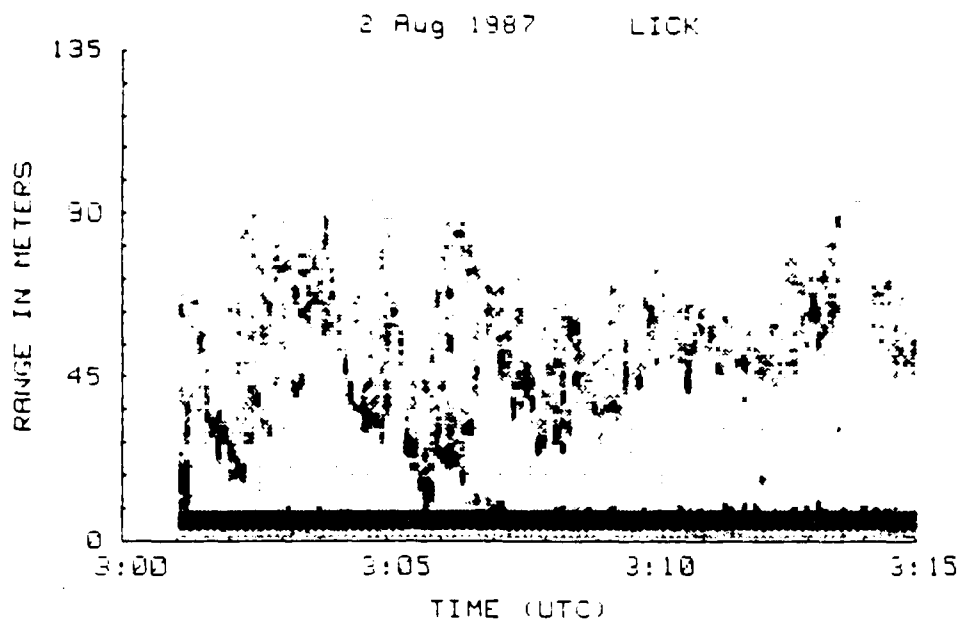


Fig. 14. Echosounder Profile; 2000 - 2015 Local Time

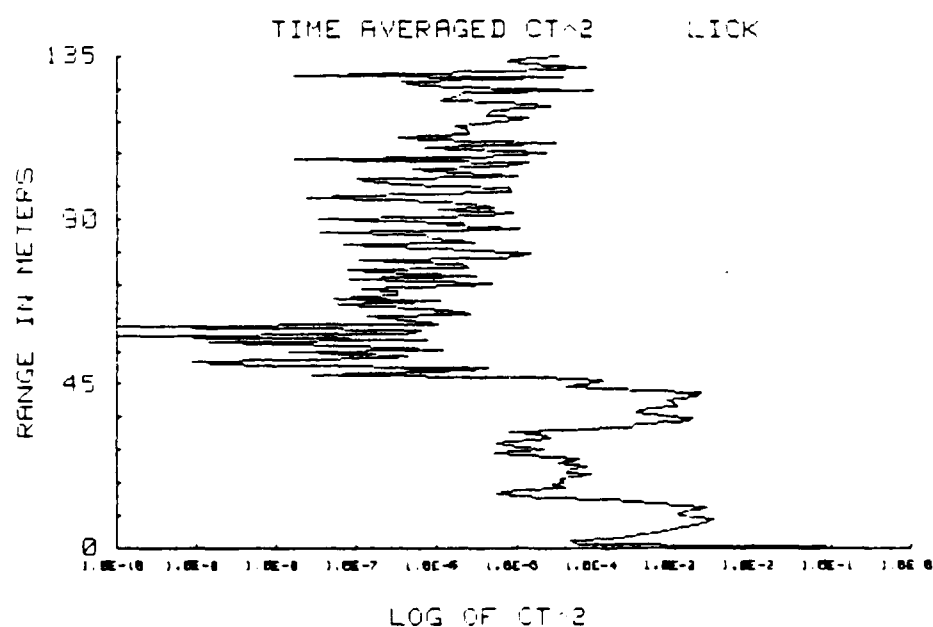
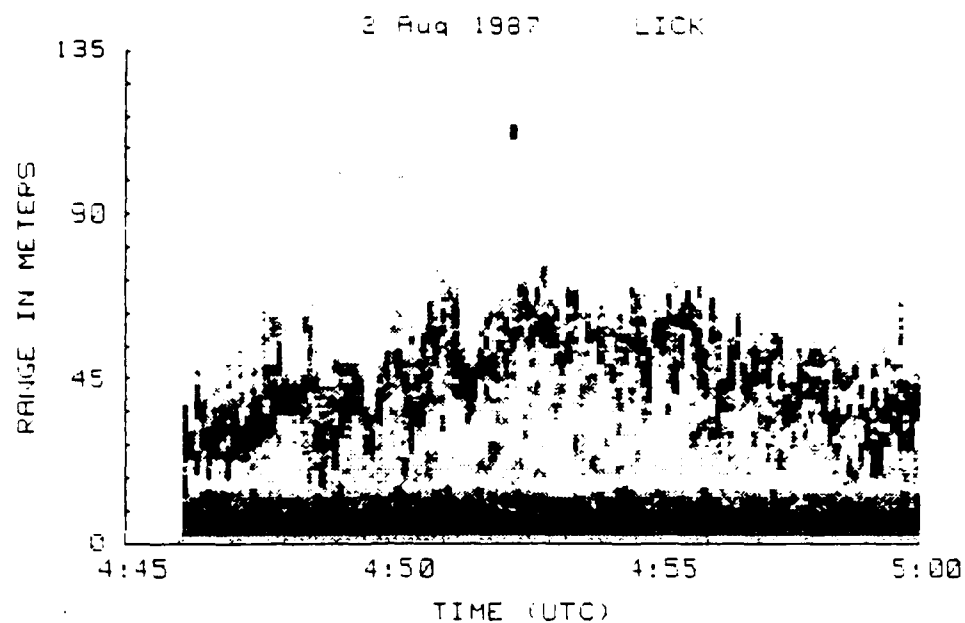


Fig. 15. Echosounder Profile; 2145 - 2200 Local Time

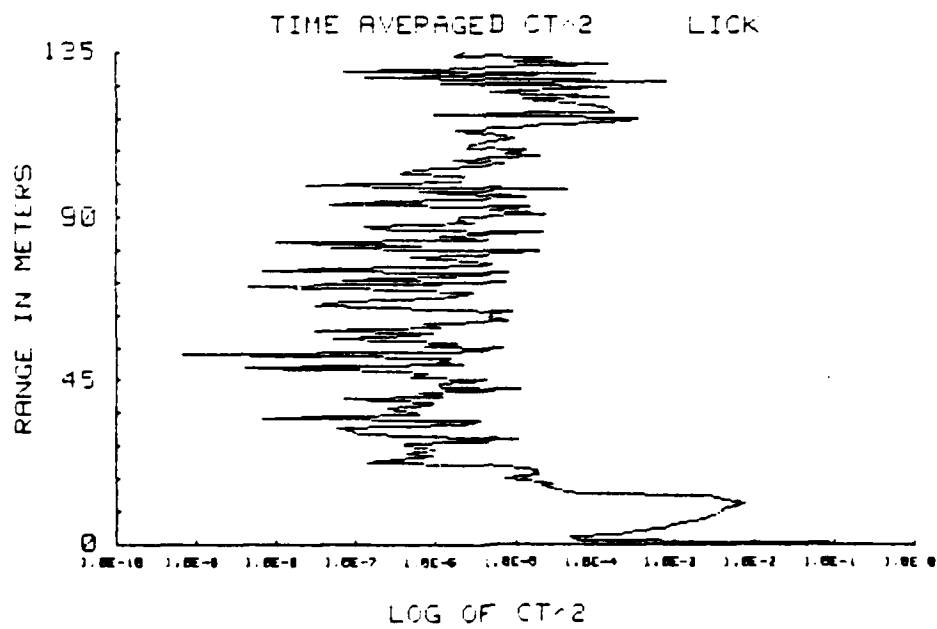
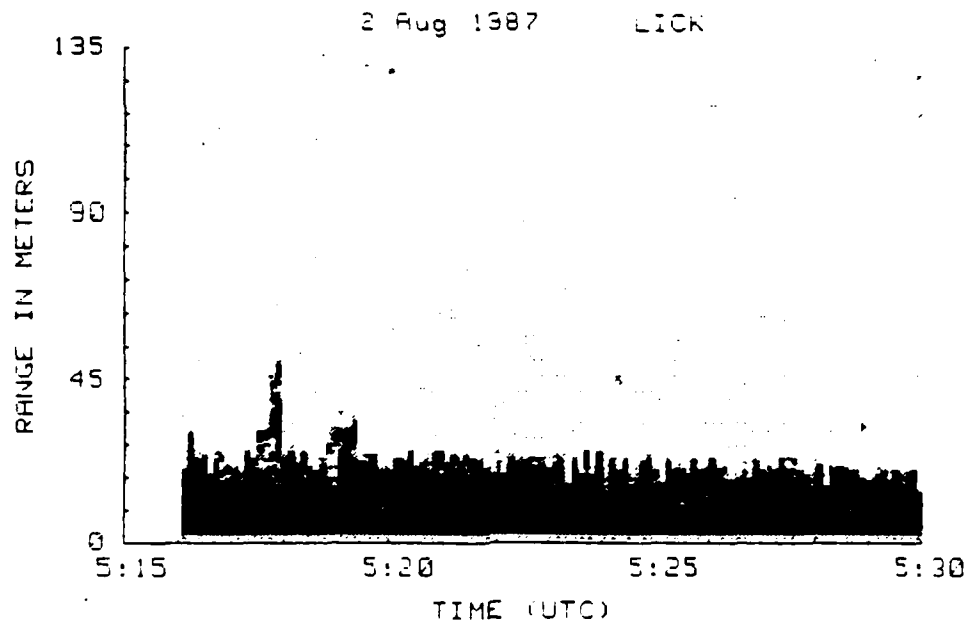


Fig. 16. Echosounder Profile; 2215 - 2230 Local Time

Early in the morning (Fig. 17) another strong layer is noted. As the sun begins to rise (Fig. 18), commencement of the daily convective pluming becomes clearly evident. These figures illustrate the dramatic ability of the high frequency echosounder to profile low level turbulence in the atmosphere. Interestingly, whenever a turbulence structure was detected on the profiler, there was also noticeable degradation to both the optical instruments in use.

The next occasion to use the echosounder occurred on 6 and 7 November 1987 with a field trip to Mt. Wilson Observatory. Unfortunatley, no echosounder data could be obtained due to severe radio frequency [RF] interference from approximately 10 radio/TV transmitters co-located at the observatory. The trip was not a loss, however, as it was used to correct a subtle flaw in the design of the pre-amp.

The problem was traced to the 'floating point ground' design of the pre-amp. The coaxial cables leading to the pre-amp made ideal antennas at the 200 megahertz range, transferring enough radio frequency voltage into the pre-amp casing to influence the

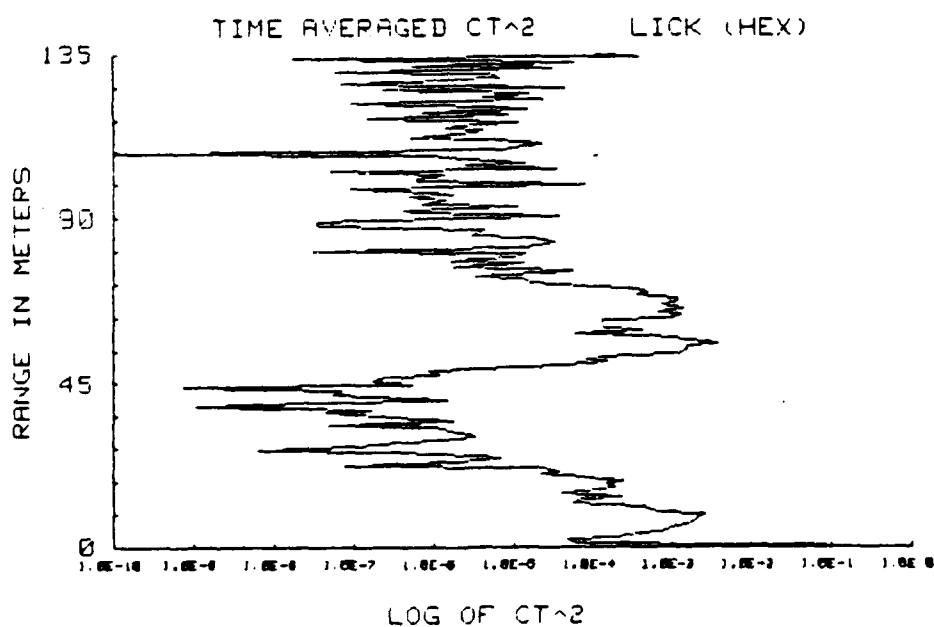
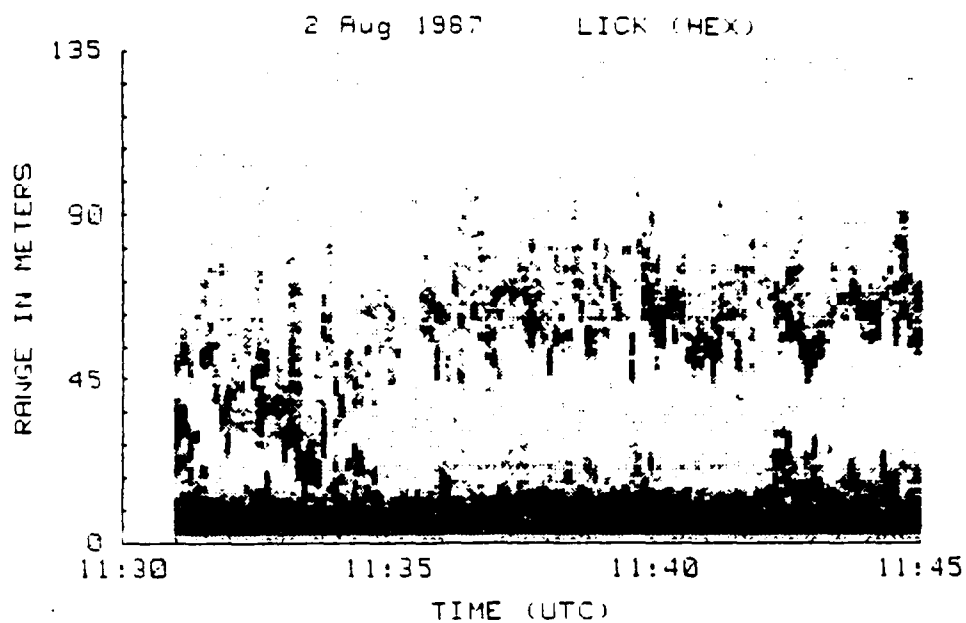


Fig. 17. Echosounder Profile; 0430 - 0445 Local Time

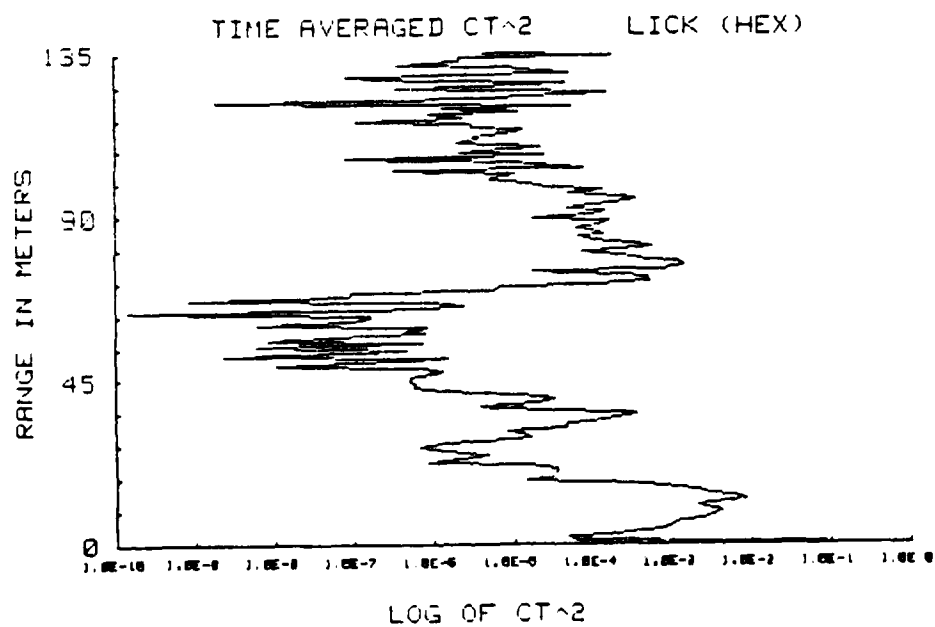
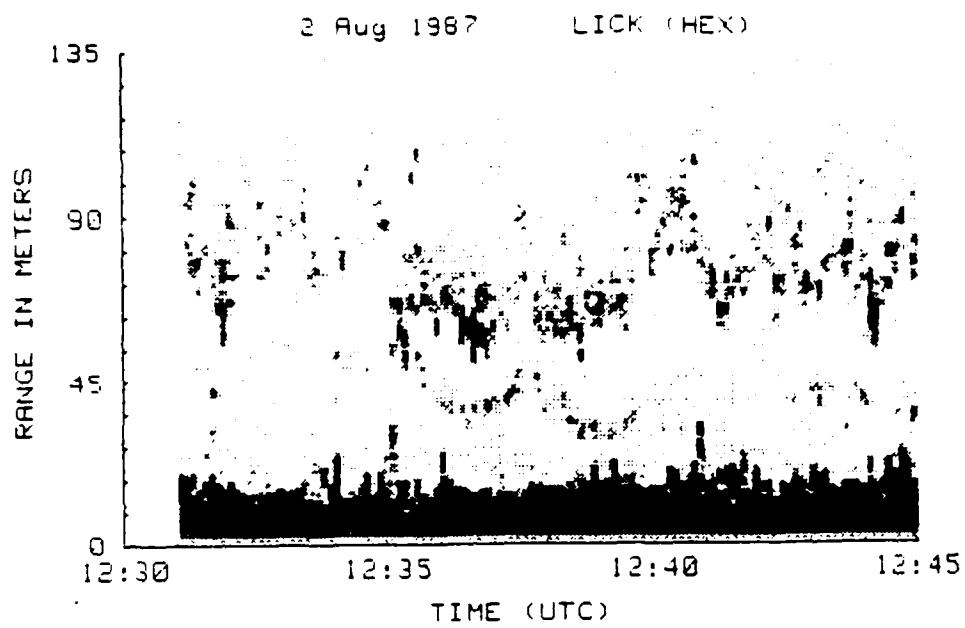


Fig. 18. Echosounder Profile; 0530 - 0545 Local Time

circuit. The rectified voltage effectively overloaded the first stage amplifier, overriding the weak return signal from the array and destroying the data. This effect went undetected in previous use of the pre-amp. The problem was corrected by improving the grounding structure of the device.

Note that all these profiles were taken with the hexagonal array mounted in the square shroud, as the hexagonal shroud was not yet completed. To ensure that the quality of data was not compromised, the square array was also run at the site and the profiles were identical.

## V. ANTENNA BEAM PATTERN MODEL

This thesis also modeled the planar acoustic array as an optical aperture, obtaining the Fourier transform of the far field 'diffraction' pattern via computer calculations. The technique rests on the fact that

"... the Fraunhofer diffraction pattern is the Fourier transform of the field distribution across the aperture ...". [Ref. 18, p. 412]

The quote applies to electromagnetic radiation, but Dr. walters correctly construed the electromagnetic amplitude as an acoustic pressure, obtaining the following equation;

$$(6) \quad P(k_x, k_y) = 1/iR \iint_{\text{aperture}} P(x, y) \exp \{i (k_x x + k_y y)\} dx dy ;$$

- $P(k_x, k_y)$  is the pressure distribution in the image plane,
- $k_x$  and  $k_y$  are the spatial frequencies along the x and y axes of the aperture respectively;  $k_j = k^* J / R$ , where  $J = x$  or  $y$ ;  $k = 2\pi / \lambda$ ,
- $P(x, y)$  is the pressure amplitude at the aperture,
- $\exp \{i (k_x x + k_y y)\}$  is the spatial variation of the aperture and
- $R$  is the distance to the image plane;  $i$  accounts for temporal phase distributions across the aperture.



The model can be thought of as a plane coherent acoustic wave passing through the aperture, which produces a diffraction pattern (the Fourier transform) in the far field (the image plane) by means of the Huygens-Fresnel principle. From this pattern it was possible to reasonably predict the size of the main lobe and the approximate angles and intensities of the side lobes. This modeling was done for both the square array and the more densely packed hexagonal array. The results are presented in this chapter.

#### A. HARDWARE

The computer used in this phase was a Hewlett Packard (HP) 217 with an INFOTEK Basic compiler, identical to the computer used in the echosounder arrangement. The memory requirements for this program, however, were tremendous, requiring over 4 megabytes of memory when using the 512 x 512 grids. This led to insertion of 2 additional memory boards into the computer, (one from INFOTEK and one from EVENTIDE), bringing the hard memory to over 5 megabytes.

## B. SOFTWARE

The program [Appendix B] utilizes a Fast Fourier Transform (FFT) routine supplied by INFOTEK. The idea is to enter the aperture (array) as a small series of points on a huge grid. Typically the grid size would be 256 x 256 points square, and occasionally 512 x 512. The array takes up only a small center portion of this grid, approximately 40 x 40 grid points. The larger the grid field in relation to the input aperture, the better the resolution, provided the input aperture is not so small as to obscure the finer details.

The aperture area was entered digitally as a series of 'ones', signifying a uniform coherent plane wave at the aperture, with the remainder of the field entered as zeroes. The FFT routine then computed the far field Fourier transform of the array, and plotted the output intensity in relation to a gray scale. The gray scale was adjusted to encompass 3 decades of intensity.

## C. RESULTS AND ANALYSIS

A sample of the input apertures, both square and hexagonal, are shown in Figures 19 and 20. Generally, the radius

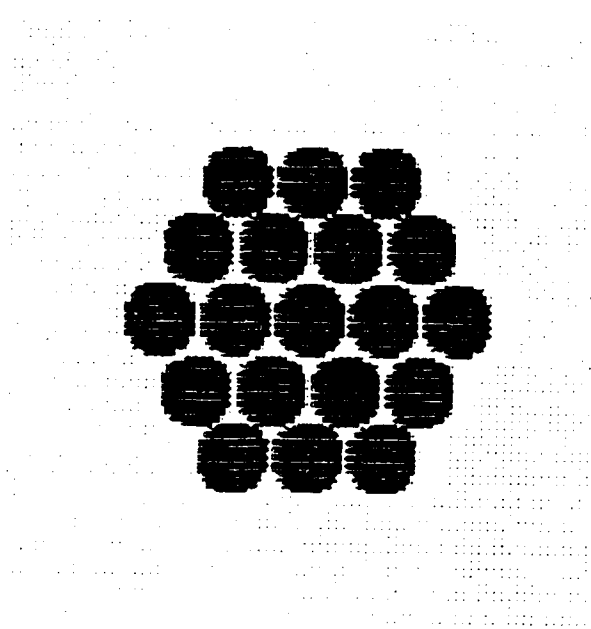


FIG. 19. HEXAGONAL ARRAY INPUT

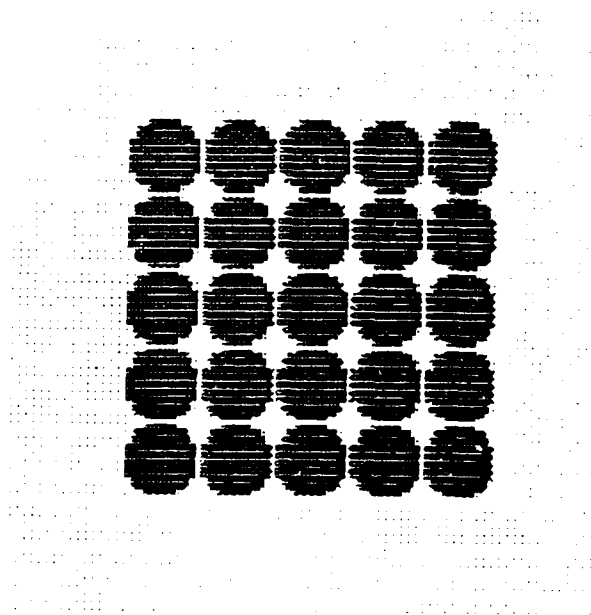


FIG. 20. SQUARE ARRAY INPUT

of each element is only 4 grid units, with a background field of 256 x 256 grid units. These figures have been enlarged to show detail. The output Fast Fourier Transform for each is shown in Figures 21 and 22 respectively. The center portion of the FFT for each array is the lowest spatial frequency for the array, and corresponds to the main lobe. Rings further out correspond to the side lobes at larger and larger angles. Rings far from the main lobe are not physical except at very high frequencies. Interestingly, as the frequency is increased, more and more side lobes are forced into the forward hemisphere.

The program calculates the beam structure of a single piston driver on an infinite plane. The actual source is not a piston driver (but the approximation is close). Huygens wavelettes propagating backwards from the end of the horns reflect from the support plane, increasing the energy of the actual lobe field. Also, the physical side lobes can extend no further than  $90^\circ$  from the axis of the array (due to surface absorption and reflection) but this limitation is ignored by the program. In addition, an obliquity factor was not

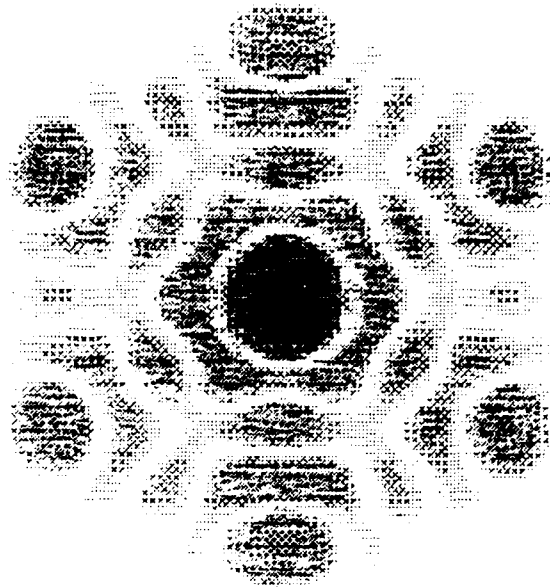


FIG. 21. HEXAGONAL ARRAY FFT OUTPUT (ENLARGED)

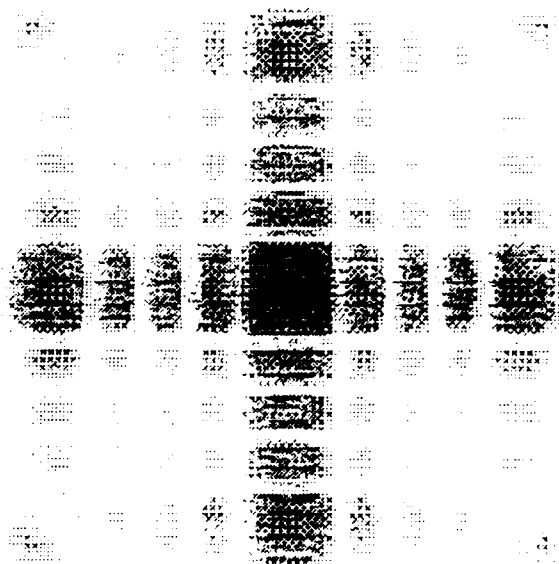


FIG. 22. SQUARE ARRAY FFT OUTPUT (ENLARGED)

included. These limitations affect the graphical output, but do not significantly affect the following calculations.

The angles of the output beam pattern rings depend on the frequency of interest (5 kHz), the dimensions of the actual array and the input/output dimension of the aperture. To calculate information from these printouts it is necessary to use optical aperture equations from Hecht and Zajac [Ref. 18]. The half angle formula for a circular aperture is:

$$(7) \quad \sin \varnothing = q/R = 1.22 L/2a \quad \text{where,}$$

- q is the distance from axis to side lobe of interest,
- a is the radius of aperture,
- L is the wavelength,
- R is the distance to the far field,
- $\varnothing$  is the half angle or cone angle from the axis to q.

The hexagonal array is not quite circular, but in the limit it approaches a circle. In this case the constant 1.22 is simply replaced by F, a constant to be determined by experiment.

By using Brigham's text [Ref. 19] it is possible to convert equation (7) into the form:

$$(8) \quad \varnothing = F \text{ ARCSIN } (L_n/N\Delta T) \quad \text{where,}$$

- $\emptyset$  is the angular measure of the side lobe from the main lobe,
- $L$  is the wavelength of interest = 6.86 cm,
- $N\Delta T$  is the total width of the sampled grid =  $(ND/X)$ ,
- $N$  is the width of the input window (grid units; 128, 256 or 512),
- $D$  is the actual dimension of the physical array (cm),
- $X$  is the dimension of the input array in grid units,
- $n$  is the output number of grid units to the side lobe of interest =  $(rz/w)$ ,
- $r$  is the distance to the output side lobe of interest (cm),  
{NOTE:  $X$  and  $D$  must correspond;  $r$  and  $n$  must correspond},
- $z$  is the width of the output window in grid units ( $\leq N/2$ ),
- $w$  is the width of the input and output windows in centimeters.

As an example, consider Figure 23. For this example,  $D = 38.735$  cm (measured between the outer edges of the farthest 2 speakers),  $w = 10.3$  cm,  $N = 256$  grid points and  $z = 128$  grid points. To calculate the angular extent of the main lobe in real space, first measure the distance (in cm) from the corner of the output quadrant to the edge of the main lobe, along the horizontal axis (Fig. 23). Here,  $r = 0.7$  cm and  $X = 40$  grid points. Therefore, equation (8) becomes:

$$(9) \quad \emptyset = F \times \text{ARCSIN} \frac{(6.86)(0.7)(128/10.3) \text{ cm}}{(256)(38.735)/40 \text{ cm}} = F \times 13.9^\circ$$

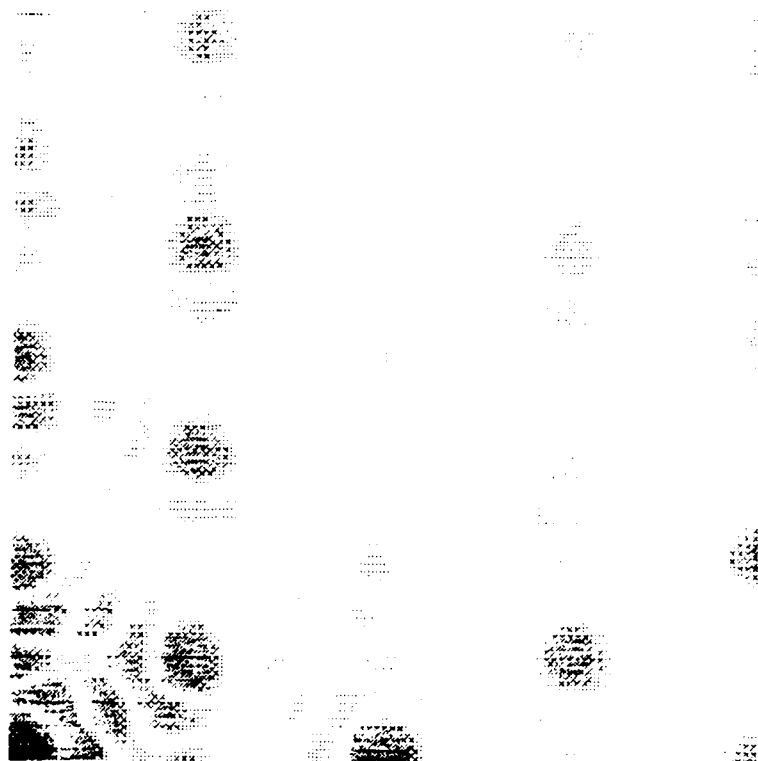


Figure 23. Output Quadrant of Hexagonal FFT

The half-angle of the actual array is only  $12^\circ$  as measured on Figure 8. This means that  $F \approx 0.86$  or  $1/F \approx 1.16$  which is very close to 1.22. Using the value  $F = 1.16$ , then the  $90^\circ$  point can be calculated for the output field. In this case,

$$(10) \quad \sin \{(1.16)(90^\circ)\} \frac{(256)(38.735)}{(6.86)(128/10.3)(40)} = r = 2.81 \text{ cm},$$



which means everything outside the corner radius of 2.81 cm can be ignored as it is non physical.

The output FFT's were correlated to the actual lobe patterns of Figures 7 and 8, the apex and side mounted patterns for the hexagonal array, and the results are plotted in Figures 24 and 25 and tabulated in Table 1. The amplitudes were normalized by assigning a value of unity to the main lobe; the angles are measured counter-clockwise from the standard X axis; the amplitude scale is in decibel units.

The measured amplitude was calculated using  $\text{INVLOG (dB/20)}$ , where 'dB' is the normalized decibel level estimated from Figures 7 and 8. The computed amplitudes relied on the formula  $20 \text{ LOG "Q/Max"}$  [see Appendix B, lines 1390 and 2380 for definitions of Q and Max].

The angles were computed using a simpler form of equation (8);

$$(11) \quad \theta = \text{ArcSin} \{ (K-1) L/N\Delta t \}, \quad \text{where } K \text{ is an index from } 1 \text{ to } N/2, \text{ and essentially allows the computation of the angle at each grid point chosen. The measured angles were taken directly from Figures 7 and 8.}$$

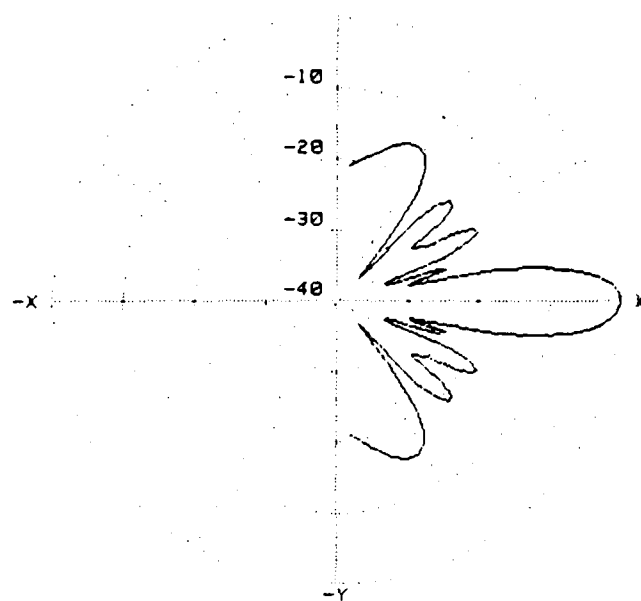


Fig. 24. Polar Plot of Apex Mounted Hexagonal Array

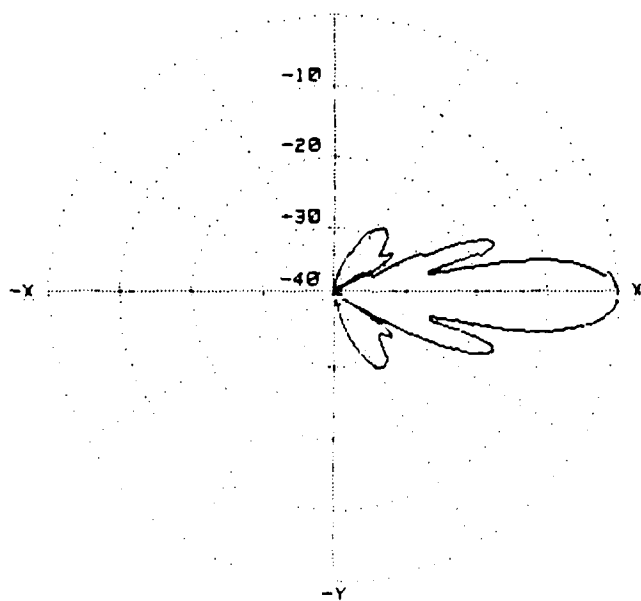


Fig. 25. Polar Plot of Side Mounted Hexagonal Array

TABLE 1. COMPARISONS BETWEEN ACTUAL LOBE PATTERNS AND  
COMPUTED LOBE PATTERNS.

APEX MOUNT ( Fig. 7 vs. 24 )

	Measured		Computed	
	<u>Ø</u>	<u>amplitude</u>	<u>Ø</u>	<u>amplitude</u>
1 <sup>st</sup> min	11°	.025	12°	.002
1 <sup>st</sup> max	16°	.126	17°	.128
2 <sup>nd</sup> min	21°	.056	23°	.007
2 <sup>nd</sup> max	26°	.095	28°	.108
3 <sup>rd</sup> min	33°	>.01	38°	.006
3 <sup>rd</sup> max	42°	.056	41°	.027
4 <sup>th</sup> min	51°	.018	46°	.007
4 <sup>th</sup> max	64°	.056	62°	.148

SIDE MOUNT ( Fig. 8 vs. 25 )

	Measured		Computed	
	<u>Ø</u>	<u>amplitude</u>	<u>Ø</u>	<u>amplitude</u>
1 <sup>st</sup> min	12°	.050	14°	.048
1 <sup>st</sup> max	18°	.158	19°	.151
2 <sup>nd</sup> min	27°	>.01	28°	.01
2 <sup>nd</sup> max	35°	.039	36°	.030
3 <sup>rd</sup> min	52°	>.01	46°	.024
3 <sup>rd</sup> max	61°	.025	56°	.029

The side mounted section corresponded to measurements along the X axis, and the apex to measurements along the Y axis. The error of the measurements was grossly estimated as approximately 10% for the minimums, as they tended to be obscured, and 3% or less for the maximums. Some values exceed this amount considerably and require further investigation.

Generally, however, the tabulated values agree strongly and suggest that this technique has considerable credibility at predicting side lobe structures of untested arrays.

## VI. CONCLUSIONS

This thesis demonstrated that increasing acoustic planar array speaker density from 25 speakers/1452 cm<sup>2</sup> ( $1.72 \times 10^{-2}$  speakers/cm<sup>2</sup>) to 19 speakers/943 cm<sup>2</sup> ( $2.02 \times 10^{-2}$  speakers/cm<sup>2</sup>) effectively suppressed the lobe spreading from a 70° cone angle to less than a 45° cone angle, with a reduction in side lobe intensity of between 4 and 10 dB.

Graphical profiles demonstrated the great variability and volatility of turbulence structures in the atmosphere and underline the need for better tools to measure and understand this structure. These profiles identify gravity waves, thermal plumes, boundary layers and other temperature induced structures. Particular important, this device allowed tentative quantification of altitude, thickness and relative intensity of mountain boundary layers over a potential DOD laser site.

Independent verification of the  $C_T^2$  values is important and is currently under study. It will further enhance the utility of this device. Due to the strong exponential dependence of acoustic

attenuation ( $\beta$ ) with increasing frequency, future improvements should also include lower frequency drivers (2-3 kHz) of similarly high efficiency, to improve the range of the device.

It was shown that acoustic array beam patterns could be successfully modeled on a computer by means of a Fast Fourier Transform algorithm and tested for optimal design. Future improvements to this technique include a method to stochastically simulate turbulence and model the beam structure as it passes through this artificial turbulence. Calculation of main lobe energy versus total energy for various arrays should also be studied.

## APPENDIX A

### List of Material Sources

Disclaimer: These sources are listed only in case exact duplication of this thesis is required at some future date. Other equally competitive sources for each item do exist and their exclusion is not a reflection of product quality in any way.

#### Barium impregnated foam:

1. Barrier Corp.  
Tigard, Oregon  
(503) 639-4192  
POC: Mark Dove

2. Latchford Corp.  
(714) 734-3660  
POC: Tom Pelligreeni

#### Cylindrical Enclosure:

1. Rubbermaid, Inc.  
1147 Akron Rd  
Wooster, Ohio 44691  
(216) 264-6464

2. Traffic Products Co.  
Citrus Heights, Ca  
(916) 723-2958  
POC: Michael Fish

#### Speakers:

Motorola Inc.  
4800 Alameda Blvd N.E.  
Albuquerque, N. M. 87113  
(505) 822-8801

#### Temperature/humidity Indicator

Weathermeasure  
P.O. Box 41039  
Sacramento, CA 95841  
(916) 481-7565

## APPENDIX B

### Fast Fourier Transform Program

```
10  ! Program plots either the input points, the FFT or the
    ! Polar Plots of a 19 element hexagon array or a 25
20  ! element square array.
30  ! This program is interactive.
40  ! diw Dec. 19, 86/LRM modified in OCT 87
50  COM Real(1:512),Im(1:512)
60  INTEGER M,N
70  DIM Real(512,512),Imag(512,512)
80  REAL Amp(100),Ang(100)
90  !
100 PRINT "ENTER THE GRID SIZE N: N= 512,256 OR 128"
110 INPUT N
120 PRINT
130 !
140 N2=N/2
150 M=LOG(N)/LOG(2)
160 !
170 PRINT "ENTER '1' TO SEE THE 19 ELEMENT HEXAGON."
180 PRINT "ENTER '2' TO SEE THE 25 ELEMENT SQUARE."
190 INPUT X
200 PRINT
210 PRINT
220 PRINT "ENTER '1' TO SEE A PLOT OF THE INPUT POINTS"
230 PRINT "ENTER '2' TO SEE A PLOT OF THE FFT"
240 PRINT "ENTER '3' TO SEE A POLAR PLOT OF INTENSITY"
250 INPUT A
260 PRINT
270 PRINT
280 PRINT "ENTER THE GRID SIZE OF EACH ELEMENT, R."
290 PRINT " USUALLY R=4 OR 8."
300 INPUT R
310 PRINT
320 PRINT
330 PRINT "ENTER '7' TO SEE THE FIRST QUADRANT ONLY"
340 PRINT " ELSE ENTER '0'."
350 INPUT C
360 ! B= THE SIZE OF THE OUTPUT WINDOW
370 B=N2/2
380 !
390 IF X=1 THEN
400 !
410 F=2.1*R*COS(.5235988)
420 FOR I=N2-6*R TO N2+6*R
430   FOR J=N2-6*R TO N2+6*R
440     IF ((I+4*R-N2)**2+(J-N2)**2)<R*R THEN
450       Real(I,J)=1.000
```



```

460     FOR K=1 TO 4
470         Real(I+2*K*R,J)=Real(I,J)
480         Real(I+2*K*R-R,J+F)=Real(I,J)
490         Real(I+2*K*R-R,J-F)=Real(I,J)
500     NEXT K
510     FOR K=1 TO 3
520         Real(I+2*K*R,J-2*F)=Real(I,J)
530         Real(I+2*K*R,J+2*F)=Real(I,J)
540     NEXT K
550     END IF
560 NEXT J
570 NEXT I
580 I
590 END IF
600 I
610 IF X=2 THEN
620 I
630 K=N2+5*R
640 L=N2-5*R
650 FOR I=1 TO N
660     FOR J=1 TO N
670         IF I<K AND I>L AND J<K AND J>L THEN
680             Cy=N2-4*R
690             FOR P=1 TO 5
700                 Cx=N2-4*R
710                 FOR O=1 TO 5
720                     IF I<Cx+R AND I>Cx-R AND J>Cy-R AND J<Cy+R THEN
730                         IF R<R*((I-Cx)^2+(J-Cy)^2) THEN
740                             Real(J,I)=1.000
750                         END IF
760                     END IF
770                     Cx=Cx+2*R
780                 NEXT O
790                 Cy=Cy+2*R
800             NEXT P
810         END IF
820     NEXT J
830 NEXT I
840 I
850 END IF
860 PRINTER IS 701
870 I
880 I This section plots the input points only
890 I
900 IF A=1 THEN GOTO 2240
910 I
920 I THIS SECTION IS THE FAST FOURIER TRANSFORM
930 I
940 T1=TIMEDATE
950 FOR I=1 TO N
960     FOR J=1 TO N

```

```

970      Re(J)=Real(I,J)
980      Im(J)=Imag(I,J)
990      NEXT J
1000  '
1010      CALL Fft(M)
1020  '
1030      FOR J=1 TO N
1040          Real(I,J)=Re(J)
1050          Imag(I,J)=Im(J)
1060      NEXT J
1070  NEXT I
1080  '
1090      FOR J=1 TO N
1100          FOR I=1 TO N
1110              Re(I)=Real(I,J)
1120              Im(I)=Imag(I,J)
1130          NEXT I
1140      NEXT J
1150      CALL Fft(M)
1160  '
1170      FOR I=1 TO N
1180          Real(I,J)=Re(I)
1190          Imag(I,J)=Im(I)
1200      NEXT I
1210  NEXT J
1220  T2=TIMEDATE
1230  ' PRINT INT(100*(T2-T1)/60)/100,"MINUTES"
1240  '
1250  IF A=2 THEN GOTO 1960
1260  '
1270  ' This section graphs the polar plot of the FFT.
1280  '
1290  B1=N2/2
1300  B2=1
1310  ' D= The actual dimension of the array(cm)
1320  D=38.735
1330  Pmax=(1+INT(D*N/(68.6*R)))
1340  '
1350  ' The 'K' loop does the side and apex mounts
1360  '
1370  R1=Real(1,1)
1380  Ia=Imag(1,1)
1390  Max=SQR(R1*R1+Ia*Ia)
1400  '
1410  FOR K=1 TO 2
1420  '
1430  IF X=1 AND K=1 THEN
1440      PRINT "                HEXAGONAL ARRAY, SIDE MOUNTED"
1450  END IF
1460  IF X=1 AND K=2 THEN
1470      PRINT "                HEXAGONAL ARRAY, APEX MOUNTED"

```

```

1480 END IF
1490 IF X=2 AND K=1 THEN
1500     PRINT "                SQUARE ARRAY, SIDE MOUNTED"
1510 END IF
1520 !
1530 ! This section computes the apex square array
1540 !
1550 IF X=2 AND K=2 THEN
1560     PRINT "                SQUARE ARRAY, APEX MOUNTED"
1570 ! The 'L' loop does only the apex mounted square
1580     FOR L=1 TO N2
1590         R1=Real(L,L)
1600         G=Imag(L,L)
1610         Q=SQR(R1*R1+G*G)
1620         IF L>Pmax THEN GOTO 1660
1630         Amp(L)=Q/Max
1640         Ang(L)=ASN(((L-1)*68.6*R)/(D*N))*180/PI
1650 !     PRINT L,Q/Max,ASN(((L-1)*68.6*R)/(D*N))*180/3.1415927
1660     NEXT L
1670 CALL Polarplt(Amp(*),Ang(*),Pmax)
1680 IF X=2 THEN GOTO 2590
1690 END IF
1700 !
1710 !
1720 FOR I=1 TO B1
1730     FOR J=1 TO B2
1740         IF B1=1 THEN P=J
1750         IF B2=1 THEN P=I
1760         R1=Real(I,J)
1770         G=Imag(I,J)
1780         Q=SQR(R1*R1+G*G)
1790         IF P>Pmax THEN GOTO 1840
1800         Amp(P)=Q/Max
1810         Ang(P)=ASN(((P-1)*68.6*R)/(D*N))*180/PI
1820 !     PRINT P,Q/Max,ASN(((P-1)*68.6*R)/(D*N))*180/3.1415927
1830     NEXT J
1840 NEXT I
1850 !
1860 CALL Polarplt(Amp(*),Ang(*),Pmax)
1870 !
1880 B2=B1
1890 B1=1
1900 NEXT K
1910 !
1920 IF A=3 THEN GOTO 2590
1930 !
1940 ! This section centers the FFT onto the output grid.
1950 !
1960 IF C=7 THEN ! USE ONLY TO GET ONE QUADRANT OF THE GRID
1970     GCLEAR
1980     GINIT

```

```

1990     GRAPHICS ON
2000     VIEWPORT 30,130,0,100
2010     WINDOW 1,N2,1,N2
2020     B1=N2-1
2030     B2=0
2040     GOTO 2340
2050 END IF
2060 '
2070 ' This section centers the output.
2080 '
2090 FOR I=1 TO N2-1
2100     FOR J=1 TO N2-1
2110         R1=Real(I,J)
2120         Ia=Imag(I,J)
2130         Real(N2+I-1,N2+J-1)=R1
2140         Real(N2-I,N2+J-1)=R1
2150         Real(N2-I,N2-J)=R1
2160         Real(N2+I-1,N2-J)=R1
2170         Imag(N2-I,N2-J)=Ia
2180         Imag(N2+I-1,N2-J)=Ia
2190         Imag(N2+I-1,N2+J-1)=Ia
2200         Imag(N2-I,N2+J-1)=Ia
2210     NEXT J
2220 NEXT I
2230 '
2240 B1=B
2250 B2=B
2260 '
2270 GCLEAR
2280 GINIT
2290 GRAPHICS ON
2300 '
2310 VIEWPORT 30,130,0,100
2320 WINDOW N2-B,N2+B,N2-B,N2+B
2330 '
2340 FOR I=N2-B1 TO N2+B2
2350     FOR J=N2-B1 TO N2+B2
2360         R1=Real(I,J)
2370         Ia=Imag(I,J)
2380         Q=SQR(R1*R1+Ia*Ia)
2390         IF A=1 THEN
2400             Z=(12*Q+1)/16 ' USE ONLY FOR PLOTTING INPUT POINTS
2410         END IF
2420         IF A=2 THEN
2430             Z=1+LGT(Q/Max)/20 ' ONLY FOR DECADE INTENSITY SPREAD
2440         END IF
2450         IF Z=0 THEN Z=0
2460         IF Z=1 THEN Z=1
2470         AREA INTENSITY Z,Z,Z
2480         MOVE I,J
2490         RECTANGLE 1,1,FILL

```

```

2500     NEXT J
2510  NEXT I
2520  !
2530  PRINT "The size of the output window is",B,"X",B
2540  PRINT "The size of the input window is",N,"X",N
2550  PRINT "The radius of each element is ",R
2560  !
2570  ! Pause statements allow insertion of parameters w/o
2580  ! redoping the FFT calculations.
2590  PRINTER IS CRT
2600  PAUSE
2610  PAUSE
2620  END
2630  !
2640  ! This section is the FFT subroutine (from INFOTEK).
2650  !
2660  SUB Fft(INTEGER M)
2670  COM Re(1:512),Im(1:512)
2680  ! FFT SUBROUTINE FROM INFOTEK 29 AUG, 1985:
2690  ! USE COMMON FOR FASTER EXECUTION 3.09 sec vs 3.59
2700  INTEGER I,J,K,L,N,Ip,Le,Le1
2710  N=2*M
2720  J=1
2730  FOR I=1 TO N-1
2740    IF I<J THEN
2750      T=Re(J)
2760      Re(J)=Re(I)
2770      Re(I)=T
2780      T=Im(J)
2790      Im(J)=Im(I)
2800      Im(I)=T
2810    END IF
2820    K=N DIV 2
2830    WHILE K<J
2840      J=J-K
2850      K=K DIV 2
2860    END WHILE
2870    J=J+K
2880  NEXT I
2890  Le=1
2900  FOR L=1 TO M
2910    Le1=Le
2920    Le=Le+Le
2930    Ure=1
2940    Uim=0
2950    Ang=PI/Le1
2960    Wre=COS(Ang)
2970    Wim=SIN(Ang)
2980    FOR J=1 TO Le1
2990      FOR I=J TO N STEP Le
3000        Ip=I+Le1

```

```

3010      Tre=Re(Ip)*Ure-Im(Ip)*Uim
3020      Tim=Re(Ip)*Uim+Im(Ip)*Ure
3030      Re(Ip)=Re(I)-Tre
3040      Im(Ip)=Im(I)-Tim
3050      Re(I)=Re(I)+Tre
3060      Im(I)=Im(I)+Tim
3070      NEXT I
3080      T=Ure*Wre-Uim*Wim
3090      Uim=Ure*Wim+Uim*Wre
3100      Ure=T
3110      NEXT J
3120      NEXT L
3130      Npscale=1./N
3140      MAT Re= (Npscale)*Re
3150      MAT Im= (Npscale)*Im
3160  SUBEND
3170  '
3180  ' This section is the polar plot subroutine written
3190  ' by Paul Davison.
3200  '
3210  SUB Polarplt(Amp(*),Ang(*),Pmax)
3220  REM *****
3230  REM THIS MODULE MAPS THE CALCULATED, NORMALIZED
3240  REM DSCS AFRAY DS(*) ON LOG NORMAL POLAR PLOTS.
3250  REM *****
3260  '
3270  ' **** INITIALIZING THE PLOTTER *****
3280  '
3290  GINIT
3300  PLOTTER IS CRT,"INTERNAL"
3310  GRAPHICS ON
3320  GCLEAR
3330  ' **** SCALING THE GRAPH *****
3340  '
3350  VIEWPORT 25,100,20,95
3360  SHOW -40,40,-40,40
3370  '
3380  LINE TYPE 4
3390  Ring=10
3400  AXES Ring, Ring, 0, 0, 5, 5, 2
3410  LINE TYPE 3
3420  DEG
3430  LORG 7
3440  CSIZE 3
3450  FOR R=0 TO 4
3460      LINE TYPE 1
3470      MOVE 0,R*Ring
3480      LABEL R*Ring-40
3490      LINE TYPE 3
3500      FOR Angle=0 TO 360
3510          PLOT R*Ring*COS(Angle),R*Ring*SIN(Angle)

```

```

3520     NEXT Angle
3530     PENUP
3540     NEXT R
3550     FOR Angle=30 TO 150 STEP 30
3560         IF Angle<>90 THEN
3570             PLOT 40*COS(Angle),40*SIN(Angle),-2
3580             DRAW 40*COS(180+Angle),40*SIN(180+Angle)
3590         END IF
3600     NEXT Angle
3610     PENUP
3620     !
3630     LINE TYPE 1
3640     DEG
3650     FOR P=Pmax TO 1 STEP -1
3660         R=40+20*LGT(Amp(P))
3670         IF R>=0 THEN
3680             PLOT R*COS(Ang(P)),R*SIN(Ang(P))
3690         END IF
3700     NEXT P
3710     FOR P=1 TO Pmax
3720         R=40+20*LGT(Amp(P))
3730         IF R>=0 THEN
3740             PLOT R*COS(Ang(P)),-R*SIN(Ang(P))
3750         END IF
3760     NEXT P
3770     !
3780     CLIP OFF
3790     !
3800     LORG 2
3810     MOVE 40,0
3820     LABEL " X"
3830     LORG 8
3840     MOVE -40,0
3850     LABEL "-X "
3860     LORG 6
3870     MOVE 0,-40
3880     LABEL "-Y"
3890     !
3900     CLIP ON
3910     !
3920     DUMP GRAPHICS #701
3930     GRAPHICS OFF
3940     PRINT CHR$(12)
3950     SUBEND

```

## LIST OF REFERENCES

1. Tatarski, V. I., The Effects of the Turbulent Atmosphere on Wave Propagation, U. S. Department of Commerce, Washington, D. C., 1971; available from National Technical Information Service, Springfield, VA. 22161.
2. Little, C. G., "Acoustic Methods for the Remote Probing of the Lower Atmosphere," Proceedings of the IEEE, Vol. 57, pp. 571-578, 1969.
3. McAllister, L. G., "Acoustic Sounding of the Lower Troposphere," Journal of Atmospheric and Terrestrial Physics, Vol. 30, pp. 1439-1440, 1968.
4. McAllister, L. G., Pollard, J. R., Mahoney, A. R., and Shaw, P. J. R., "Acoustic Sounding - A New Approach to the Study of Atmospheric Structure," Proceedings of the IEEE, Vol. 57, pp. 579-587, 1969.
5. Asimakopoulos, D. N., Cole, R. S., Caughey, S. J., and Crease, B. A., "A Quantitative Comparison Between Acoustic Sounder Returns and the Direct Measurement of Atmospheric Temperature Fluctuation," Boundary Layer Meteorology, Vol. 10, pp. 137-147, 1976.
6. Mouldsley, T. J., Cole, R. S., Asimakopoulos, D. N. and Caughey, S. J., "Simultaneous Horizontal and Vertical Acoustic Sounding of the Atmospheric Boundary Layer," Boundary Layer Meteorology, Vol. 17, pp. 223-230, May 1979.
7. Weingartner, Frank J., Development of an Acoustic Echosounder for Detection of Lower Level Atmospheric Turbulence, Master's Thesis, Naval Postgraduate School, Monterey, California, June 1987.



8. Wroblewski, Michael R., Development of a Data Analysis System for the Detection of Lower Level Atmospheric Turbulence with an Acoustic Sounder, Master's Thesis, Naval Postgraduate School, Monterey, California, June, 1987.
9. Walters, D. L., "Atmospheric Modulation Transfer Function for Desert and Mountain Locations: the Atmospheric Effects on  $r_0$ ," Journal of Optical Society of America, Vol. 71, No. 4, pp. 397-405, April 1981.
10. Walters, D. L., "Atmospheric Modulation Transfer Function for Desert and Mountain Locations:  $r_0$  Measurements," Journal of Optical Society of America, Vol. 71, No. 4, pp. 406-409, April 1981.
11. Walters, D. L., Saturation and the Zenith Angle Dependence of Atmospheric Isoplanatic Angle Measurements, paper presented at the SPIE Conference, April 1985.
12. Neff, W. D., "Quantitative Evaluation of Acoustic Echoes from the Planetary Boundary Layer," NOAA Technical Report ERL 322-WPL 38, June 1975.
13. Probert-Jones, J. R., "The Radar Equation in Meteorology," Quarterly Journal of the Royal Meteorology Society, v. 88, pp. 485-495, 1962.
14. Hall Jr., F. F., and Wescott, J. W., "Acoustic Antennas for Atmospheric Echo Sounding," Journal of the Acoustical Society of America, Vol. 56, No. 5, pp. 1376-1382, November 1974.
15. Fuller, Robert J., Parametric Analysis of Echosounder Performance, Master's Thesis, Naval Postgraduate School, Monterey, California, September, 1985.
16. Asimakopoulos, D. N., Helmis, C. G., and Stephanou, G. J., "Atmospheric Acoustic Minisounder," Journal of Atmospheric and Oceanic Technology, Vol. 4, pp. 345-347, June 1987.

17. Butler, John D., Development, Validation and Use of a Computer-Controlled System for the Investigation of Phase and Amplitude Shaded Acoustic Arrays, Master's Thesis, Naval Postgraduate School, Monterey, California, December, 1986.
18. Hecht, Eugene, and Zajac, Alfred, Optics. Massachesetts: Addison-Wesley Publishing Co., Inc, 1974.
19. Brigham, E. O., The Fast Fourier Transform. Englewood Cliffs, New Jersey: Prentice-Hall, Inc., 1974.

## INITIAL DISTRIBUTION LIST

	No. of Copies
1. Defense Technical Information Center Cameron Station Alexandria, VA 22304-6145	2
2. Library, Code 0142 Naval Postgraduate School Monterey, CA 93943-5002	2
3. Prof. Donald L. Walters Department of Physics (Code 61We) Naval Postgraduate School Monterey, CA 93943-5004	5
4. Prof. Steven L. Garrett Department of Physics (Code 61Gt) Naval Postgraduate School Monterey, CA 93943-5004	1
5. Commandant (G-PTE) U. S. Coast Guard 2100 2nd Street, S. W. Washington, D. C. 20593	2
6. Prof. Karlheinz E. Woehler Chairman, Department of Physics (Code 61Wh) Naval Postgraduate School Monterey, CA 93943-5004	1
7. Commanding Officer Surface Warfare Officers School Command Newport, RI 02841 ATTN: LT. L. R. Moxcey	1

END

DATE

FILMED

5-88

DTIC